NOVEL NEAR-FIELD MICROWAVE TESTING METHOD FOR OUTDOOR INSULATORS

A THESIS IN ELECTRICAL ENGINEERING

Master of Science in Electrical Engineering

Presented to the faculty of the American University of Sharjah
College of Engineering
in partial fulfillment of
the requirements for the degree

MASTER OF SCIENCE

by

YASSER ADEL SAKER

B.S. 2008

Sharjah, UAE

May, 2011

NOVEL NEAR-FIELD MICROWAVE TESTING METHOD FOR OUTDOOR INSULATORS

Yasser Adel Saker, Candidate for the Master of Science
American University of Sharjah, 2011

ABSTRACT

Outdoor insulators are very vital in providing energized overhead lines mechanical support and electrical insulation from grounded structures. Insulators can be divided according to the material they are made of into glass, porcelain and polymer (Non Ceramic) insulators. After the 1970's, Non Ceramic Insulators (NCI) became very popular because of their ease of manufacturing, good contamination performance (due to hydrophopecity) and low installation cost. When manufactured or stored, insulators may be subjected to defects such as air voids, cracks in the fiberglass reinforced polymer (FRP) rod and contamination inclusion in the silicone rubber matrix. So, testing the insulator before the installation process and ensuring that it is defect free is very important to provide safety for workers and to avoid power outages. Unlike porcelain and glass insulators, it is hard to detect defects in NCI due to the absence of intermediate electrodes and the close distance between the sheds.

In a previous study, a new technique was proposed that depends on near-field Microwave non destructive testing (NDT) using open ended rectangular waveguide sensor. In this technique, the NCI was considered as a multi layer structure where any defect in these layers will affect the reflection coefficient value measured by the sensor. The microwave NDT technique showed good potential in detecting different types of defects in the NCI. One of the short coming of the previous work is the lack of the ability of the system in identifying the type of defect inside the NCI sample. In this work, different defects in both silicone rubber and fibre glass core were detected. Artificial neural networks (ANNs) were applied in order to detect and specify the type of defect in the outdoor insulator. Moreover, stepwise regression was used in extracting the important features, where the features inspected in this study are Fast

Fourier Transform (FFT) components, statistical features, and the details energy of the wavelet decomposition.

The detection rate of defects in the silicone rubber layer was found to be 92.5%. Moreover, the type of defect in the silicone rubber matrix was successfully specified (air void or metal) where a classification rate of 95% was reached. In the case of fiberglass core defects, the detection rate was 90% and the classification rate between air void in the fiberglass core and cracked core samples was 97.5 %.

Table of Contents

List of Figures

List of Tables

ACKNOWLEDGEMENT

This thesis wouldn't have been possible without the help of Dr. Ayman El Hag who offered me all types of technical and spiritual support. He also taught me never to give up during my research despite the difficulties we faced. I would like to express my deep appreciation to Dr. Nasser Qaddoumi who has never stopped providing me in useful and beneficial technical guidance. I owe my deepest gratitude to my parents who eased and inspired my research process. I would also like to thank my brother and sister for providing a suitable and calm atmosphere for me. Moreover, I am very grateful to Mr. Ibrahim Abu-Seif who has not saved any effort in helping me conducting the experimental setup. At last but not least, my thankfulness goes to my colleagues (Ayman Al Jundi, Ibrahim Shurrab, Rida Mourtada, Refat Atef, and Abdalla Daher) who offered me big help in this work.

CHAPTER 1: Introduction

1.1 Types of Outdoor Insulators

Insulators can be divided according to the dielectric material in to porcelain, glass and polymer. Glass and porcelain insulators are called ceramic insulators while polymer insulators are called non-ceramic (NCI) or composite insulator. The most common ceramic insulator is the pin and cap type where each unit is connected to another by a metal hardware. Figure 1-1 shows glass insulators and a polymer insulator.

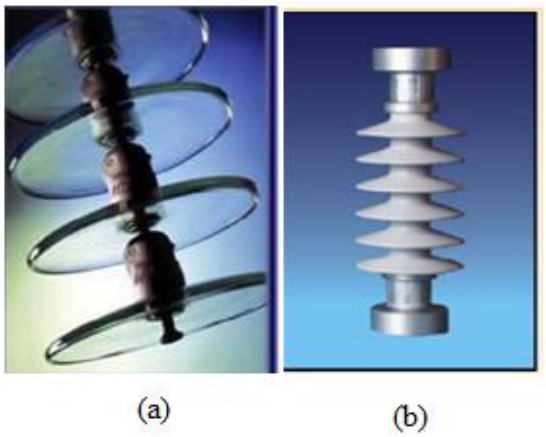

Figure 1-1 (a): glass insulator, (b): NCI [1]

Moreover, insulators can be divided according to where they are connected to the following categories:

1. Line insulators: connected to overhead lines.
2. Station Insulators: used to support the bus, enable connection between the energized terminal and the overhead line, and provides housing on measuring devices such as instrument transformers.

In addition to that, line insulators can be divided into the [1]:

1. Suspension insulators: suspending the overhead line from the conductor.

2. Line Post insulators: they are put in a tilted position.
3. Dead End insulators: used at the beginning /end of the line and in changing direction.

1.1.1 Non Ceramic Insulators

Although Non Ceramic Insulators (NCIs) are affected by aging, after 1970s NCI became the common used type of insulators because of the following mentioned reasons:

1. Better contamination performance (due to being hydrophobic).
2. Light weight.
3. Vandalism resistance.
4. Low installation and initial cost.

NCIs mainly consist of fiberglass core, weather sheds covering the core and a coupling hardware attached to the core at both ends as shown in Figure 1-2.

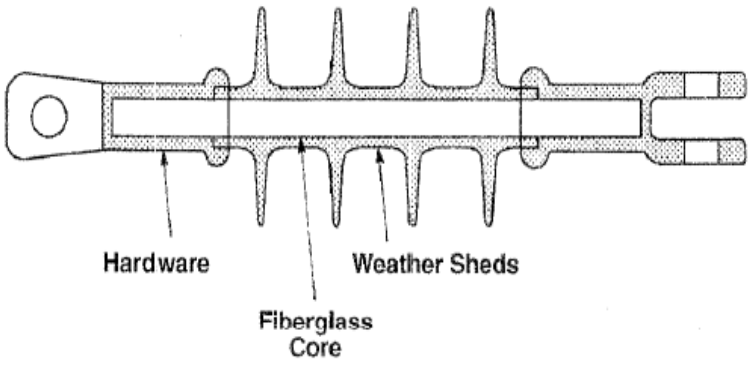

Figure 1-2: Suspension Insulator [1]

The fiberglass core acts as the main load bearing member. It has 70-75% axially aligned E-glass fibers in a reinforced resin. The resin system is either epoxy or vinyl ester where the process used for forming the rod is called pultrusion. The end fittings are either made of aluminum, malleable iron or steel. Weather sheds are made from various polymeric materials (like silicone rubber). They are shaped and spaced in a way they protect the core from contamination and moisture. Weather sheds also provide electrical insulation between the two end fittings [1].

1.1.2 Aging of NCIs

The presence of electrical stress with certain environmental conditions can lead to different factors that affect the aging performance of NCIs. Some of these factors are listed below [2]:

1. Electrical discharges: It is the most widely recognised cause of aging. There are two main electrical discharge activities that happen at the insulator's surface:
   a) Dry-band arcing: When the NCIs lose their hydrophobicity, a film of water develops on the surface, leading to flow of leakage current. Because of the non uniform leakage current and the heat developed, dry-bands will be formed. These dry-bands will result in arcing on the surface of the insulator.
   b) Corona: It happens when the electric field increases more than the onset value of air breakdown at the insulator's surface.
2. UV radiation: it results from sunlight, corona, and dry-band arcing. If sufficient UV energy is present, it will damage the molecular structure of silicone rubber matrix.
3. Temperature: while temperature may not cause aging, it accelerates the aging process.

1.1.3 Characterization of Aged NCIs

Aging of silicone rubber insulators due to natural and accelerated conditions has been studied extensively in the literature [1]-[4]. There are many aging tests for outdoor insulators such as: salt-fog, rotating wheel, and inclined plane tests. During these aging tests, many quantities are measured to assess the performance of NCIs. These quantities can be categorized into electrical, physical, and chemical. Some of electrical quantities measured are listed below[2]:

1. Flashover Voltage: Determines the maximum voltage that the insulator can withstand at various levels of contamination.
2. Leakage Current (LC) measurement: LC measured in the field or during the aging test. Either the maximum current value or the number of peak pulses along with their values is recorded during the aging of NCI.

Some of the physical quantities measured to assess the insulation surface conditions can be summarized as follows:

1. Hydrophobicity: the ability of silicone rubber to repel water in order to prevent formation of continuous conducting path. In the hydrophobic check, the contact angle is measured since it is an indication of the chemical composition and physical structure of the silicone rubber surface [2].
2. Surface Contamination: as the insulator ages in the field, the quantity of pollution on its surface increases. One way to quantify surface contamination is to measure the equivalent salt deposit density (ESDD). Another measured pollution parameter is the non-soluble solution density (NSDD). NSDD measures the non-ionic component in the pollution layer [2].

Finally chemical quantities are used to evaluate the insulator surface condition. Two of the most common techniques are described below:

1. Fourier transforms infra-red (FTIR) analysis: it is an important tool to detect different types of chemical bonds in organic materials. FTIR depends on the idea that different molecular bond vibrate at different frequencies which will vary the wavelength of the light absorbed by the material [4],[2].
2. X-Ray Spectroscopy: it is used to measure the chemical composition of the silicone rubber surface. With aging, there is a decrease in the concentration of silicone and Carbone. On the other hand, there is an increase in the concentration of oxygen. Moreover, there is a decrease in the silicone to filler concentration ratio [2].

1.1.4 Pre-installation problems faced by NCIs

NCIs' bad design and mishandling may cause several problems in the NCI. Some of these problems along with their causes are listed below[1]:

1. Core damage during fixing the end fittings: swaging is one of the methods used for attaching the end fittings to the core of the insulator. When swaging dies are put, the core may be cracked. In addition to that, when there is a small difference between the hardware diameter and the core diameter, swaging the end fittings may also crack the core. Another new method used for fixing the end fittings is crimping. Over crimping (applying extra force on the end fittings) may also crack the fiberglass core. These cracks are usually not detected by routine tests.

2. Mishandling: Sharp surfaces during transportation, ropes and slings when lifting the NCI may damage the insulator. Cantilever and torsion loads during installation may crack the core. When a damage of the housing occurs, moisture and voltage can result in either tracking, permanent conducting path across the surface of the insulator, or brittle fracture of the fiber glass core. Usually tracking of the core takes a long time according to the location of the damage, wetting contamination level. Brittle fracture has more possibility to happen when the defect is near the end of the NCI and it happens as a result of the acids formation during corona discharge in the presence of moisture. This can result in line drop.
3. Bonding: sometimes the bonding between the core and the polymer housing is not sufficient due to incorrect preheat temperature, moisture, or incorrect mold temperature. This may cause tracking and puncture along the unbounded interface.

1.1.5 Testing Techniques for NCIs

Installing defected outdoor insulator increases the possibility of outages in the network. That's why, testing outdoor insulators before installation is very crucial. As mentioned in [1], prior to installation some testing methods on defected NCI samples has been studied. The types of defects tested are cracked rods soaked in water prior to assembly, silver conductive paint applied to rod prior to assembly, rod housing contamination, conducting wire in the rod-housing interface, rod cracked by over crimping, and metal shavings in the rod-housing interface. The testing methods employed with their effectiveness in detecting defects are mentioned below [1]:

1. Resistance Measurement: Megger is used to measure the insulation resistance. All defective NCI showed an infinite insulation resistance, so this method was considered ineffective.
2. Partial discharge (PD) measurements resulted in detecting only insulators that include copper wires in the rod housing interface while other defected NCIs did not show a noticeable PD values.
3. Radio Influence Voltage (RIV): In this test, a sine wave voltage is applied across the insulator. Then, the voltage measured, in case of defected sample, is expected to be in the milli-volts range (>10 mV) at a specific radio frequency [5]. RIV was able to

detect silver painted rod, cracked rod and rod wire in the rod housing interface extending over the full insulator length. RIV failed in other defect types.

4. Voltage applied technique: the insulator was exposed to two times the service voltage for five minutes. The technique was only able to detect the copper wires extending over the whole insulator.
5. Modified hot stick tester: where a 1.8 KV voltage is applied across the two electrodes. This technique was only able to detect copper wires in the rod housing.
6. Electric field measurement: The application of the voltage across the insulator terminals result in electric field along the surface of the insulator where a field probe measures the electric field on the surface of the insulator with a capability of microprocessor recording and downloading data to computers. Several inches long of tracking along the rod-sheath, the sheath of the housing can be detected. The technique was not able to detect punctures, air voids and small dimension defects.
7. Infrared (IR) Imaging: It is based on detecting non uniform temperature rise in the insulator, where the temperature rise is associated with corona discharges and leakage current [6].

In summary, all these testing methods suffer from sensitivity to any disturbance, limited to some defects and do not provide reliable results in the case of cracked FRP rod. Moreover, IR technique can only be used when the insulator is energized. Recently, it has been found that Near-field Microwave Non Destructive Testing has a great potential in detecting damages in NCIs [7].

1.2 Testing using Near-field Waveguides Probes

Near-field waveguide imager is a 2-D intensity image that uses an open-ended waveguide as an imaging probe in order to measure the reflection coefficient along the spatial coordinates of the a structure. The main objectives behind using these Microwave Near-Field Sensors are:

a. Detecting the existence of any strange entity inside a known dielectric material.
b. Being able to define the entity type inside the dielectric material.

Near-field microwave testing is a simple nondestructive testing (NDT) technique that depends on the idea that microwaves, in the near-field regions, when propagating in a

media are very sensitive to discontinuities. In our case the discontinuities are either cracks in the fiber glass, air voids in the silicone rubber, air voids in the fiberglass core or the presence of metallic particles. These discontinuities will have different dielectric properties and hence different ability of a material to store and absorb energy. This will result in reflection of a portion of the incident field wave while the other portion will remain propagating. Non Ceramic materials are made of dielectrics and this will make it easy for the microwave to penetrate through it and according to the type of discontinuity mentioned above the magnitude and the phase of the reflected signal will vary [7].

There are many reasons that encourage using microwave NDT. Some of these reasons are demonstrated as following [7]-[12]:

1. It is simple, inexpensive and easy to use technique.
2. It is very safe for human beings to use.
3. It is very easy to manufacture since it only needs a waveguide, Gunn diode oscillator, diode detector and an amplification circuit if needed.
4. The waveguide and diode detector can easily perform well for a long time. On the other hand, the gun oscillator shall be handled carefully since it can be burned easily.
5. The system may or may not be in contact with the surface under examination.
6. The dimensions of the enclosed discontinuities may be estimated.
7. The required microwave signal power is in low milli-Watt range.
8. The technique does not cause electromagnetic noise and it is not affected by external electromagnetic interferences.

This section will contain the mathematical formulation of an N-layered structure imaging, and types of microwave near-field sensors.

1.2.1 Near-Field Properties of Rectangular Waveguides Used for Imaging

In order to understand the information contained in a near-field microwave image, it is important to know how the electric field behaves in a multilayer composite material. In this subsection, a summary of the mathematical formulation of the field in a stratified material is mentioned. Open ended waveguide probe radiating into a multilayered composite material, that resembles the discontinuities in the non ceramic insulator, is shown in Figure 1-3.

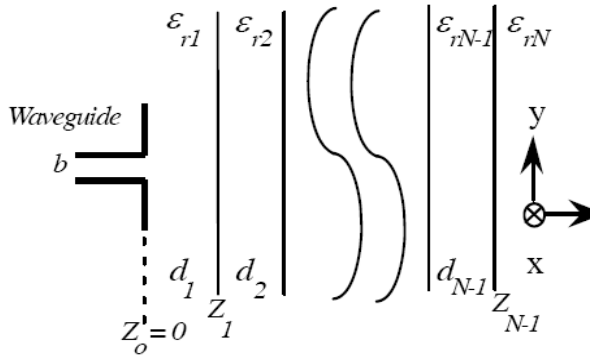

Figure 1-3: Open-ended flanged waveguide radiating in to multilayer stranded material [7]

Assuming a dominant TE_{10} mode incident on the rectangular waveguide aperture, the terminating admittance at the waveguide of an arbitrary shape is given by equation 1-1 [8]:

$$Y = G + jB = \frac{\iint [E(x,y,0)x\, W(x,y,0)]a_z\, dxdy}{(\iint [E(x,y,0).e_0(x,y)dxdy])^2} \quad (1\text{-}1)$$

Where E(x, y, 0) is the electric field at the aperture of the waveguide, $e_0(x,y)$ is the dominant mode field which is TE10 and $W(x,y,0)$ is given by:

$$W(x,y,0) = H(x,y,0) + \sum Y_n h_n(x,y) \iint [E(\delta,\eta,0).e_0(\delta,\eta,)]d\delta d\eta \quad (1\text{-}2)$$

Where:

e_n and h_n : are the nth reflected mode vectors

Y_n: is the characteristic admittance of the waveguide aperture at the nth mode

a and b: are the broad and narrow dimensions of the waveguide.

The TE_{10} mode aperture field distribution is given by equation 1-3:

$$E_y(x,y,0) = e_0(x,y) = \sqrt{\frac{2}{ab}}\cos\left(\frac{\pi x}{a}\right) \quad (1\text{-}3)$$

And $E_y(x,y,0)$ is zero outside the waveguide dimensions.

The reflection coefficient at the waveguide aperture is noticed to have a relationship with the terminating admittance of the waveguide as illustrated in equation 1-4:

$$\Gamma = |\Gamma|e^{j\theta} = \frac{1-Y}{1+Y} \quad (1\text{-}4)$$

In order to maximize the detection of any strange entity in the multi-layered structure, variations in magnitude and phase of reflection coefficient shall be maximized. This could be achieved by trying different frequencies of operation and stand-off distances for the open-ended waveguide sensor from the sample under test.

1.2.2 Types of Microwave Near-Field Sensors

As shown previously, the reflection coefficient is a complex parameter that has a magnitude and phase depending on the discontinuity type and position. Accordingly, there are three types of probes: magnitude probes, phase probes and complex probes. Phase at each (x, y) coordinates is proportional to reflection coefficient's phase variation at that point. Figure 1-4 shows an imaging scattormeter microwave circuit.

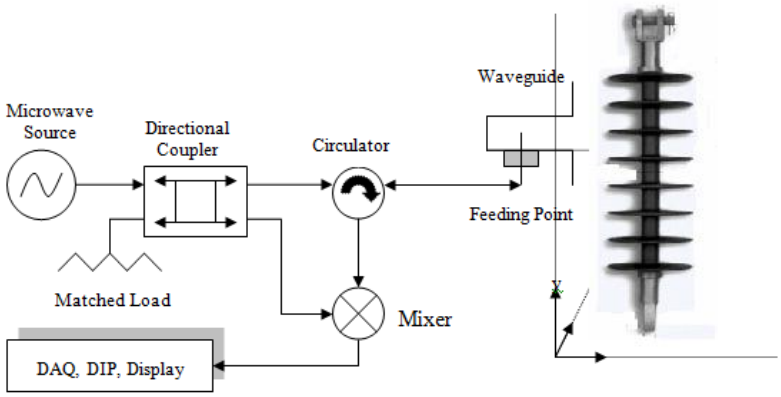

Figure 1-4: Phase Probe

The components used in phase probe circuit include:

1. Microwave oscillator, used to generate a microwave signal at a certain power and frequency.
2. Directional Coupler, used to divide the power of the microwave one used as a reference in the mixer and the other used to propagate in the dielectric material.
3. Waveguide, used to propagate the microwave signal to the material space under test where the signal will interact with the material and will experience phase shifts.
4. Circulator, used to isolate the reflected signal from the standing wave.

5. Mixer, used to mix the reflected signal with the reference signal since they both have the same frequency.

In the magnitude probes, the intensity of the reflected signal at a certain point is proportional to the magnitude of the reflection coefficient. Figure 1-5 shows the magnitude probe circuit.

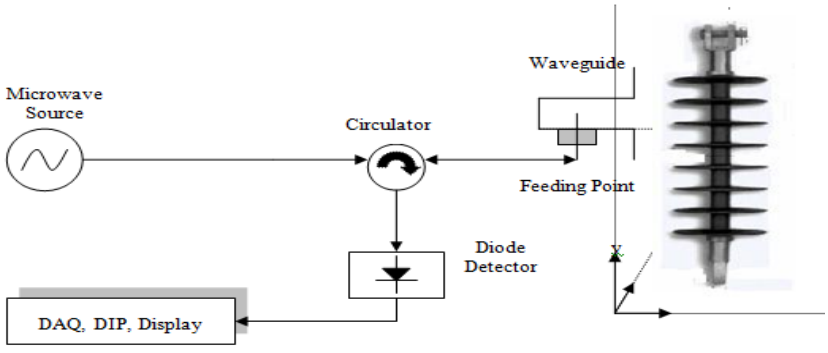

Figure 1-5: Magnitude probe

The components used for magnitude probe are a microwave oscillator, a waveguide, a circulator and a diode detector. The diode detector outputs power proportional to the magnitude of the reflection coefficient. In the complex probes, the intensity of the image is proportional to the complex reflection coefficient. Its circuit is very similar to the magnitude probe's circuit without the use of the circulator where the diode detector output will be proportional to the power of the standing wave and not the reflected signal [9].

CHAPTER 2: Materials and Methods

Since the fibreglass core manufacturers are different from the silicone rubber insulator manufactures, two separate cases were studied in this thesis. The first case concentrates on the detection and classification of defects that take place in the silicone rubber layer (air voids and metal inclusion), while the second case focuses on the detection and classification of the fibreglass defects (cracks and air voids). The methodology for both cases is the same.

In this chapter, the methodology and the tools, that are used to approach the target of this research, will be explained. After acquiring the signal from the near-field microwave sensor and storing it in a computer, digital low pass filter and a notch filter were applied. The digital filters are used in order to remove the unnecessary noise from the signal. The next step is to extract some features from the signal like: statistical features, wavelet details' energies, and the Fast Fourier Transform (FFT) components. Since most of these features are confusing the neural network and didn't give good classification rate, stepwise regression was used. Stepwise regression helped choosing the important features only. Then, Artificial Neural Network helped in deciding whether a sample has a defect or not. If the sample is defected, another ANN will be applied in order to specify the defect type. A block diagram that explains the methodology is shown in Figure 2-1.

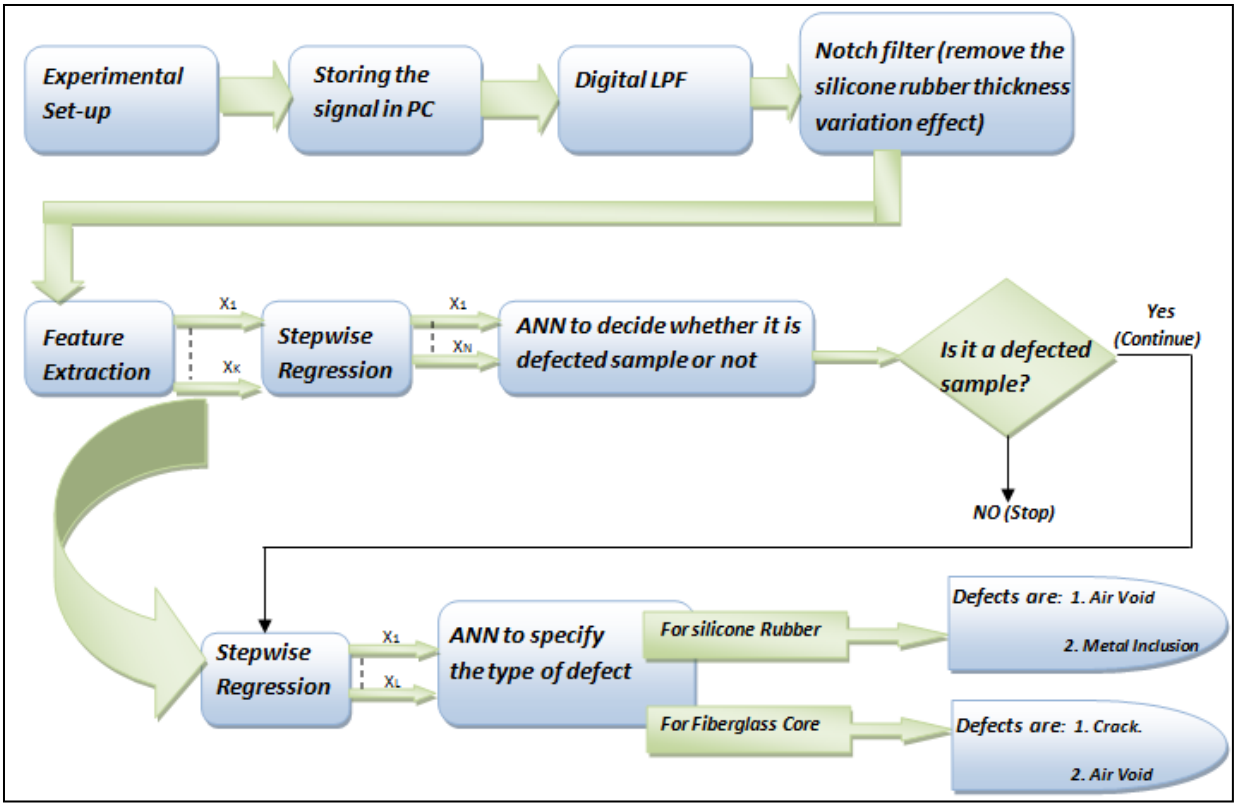

Figure 2-1: Block diagram explaining the methodology

2.1 Samples Preparation

This section explains how defected samples were prepared. The main two types of defects in the silicone rubber layer with the way they are prepared in the lab are listed below:

1. Air voids in the silicone rubber: this was modeled as a drilled hole through the silicone rubber layer, where forty different air void signals were acquired. The different samples were either of 1mm diameter or 2mm diameter. Moreover, the drills were done at different depths.
2. Conductive inclusions in the silicone rubber layer: this was implemented by inserting metallic needle in the silicone rubber layer at different depths. Forty different metal inclusion signals were acquired for this case.

After that, defected fiber glass core samples were prepared. The two types of fiberglass core defects that this thesis focused on are listed below:

1. Cracks in the fiber glass core: This was done by applying a mechanical load on the fiber glass rod. The force applied caused an internal crack and not a surface crack. forty different signals for this type of defect were obtained.
2. Air Voids in the fiber glass core: A hole in the fiber glass core was made at different depths. The diameter of these drills were either 1mm or 2mm. Similar to the case of the crack, forty signals were acquired for the fiber glass air void case.

2.2 Experimental Set-Up

In this section, the NDT near-field microwave testing setup will be explained. Figure 2-2 briefly explains how near-field microwave sensor signals are obtained.

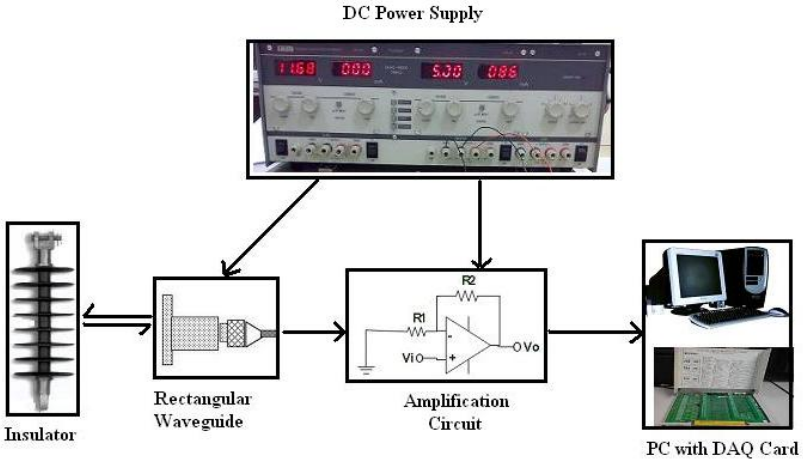

Figure 2-2: Block Diagram of Microwave Non destructive Testing [7]

As shown in Figure 2-2, the NCI sample will be scanned by a waveguide sensor. In order to scan the NCI at different locations of its circumference, NCI sample needs to be rotated. After that, the output signal measured by the waveguide sensor will be amplified by an op-amp. At the end, DAQ card will be used in order to store the data in the PC. The main components needed for this set-up are listed below:

1. Mechanical setup: it mainly consists of stand, drill heads (to hold the NCI), and ball bearing that will ease the rotation of the insulator sample as shown in Figure 2-3.

Figure 2-3: Mechanical Setup including: Drill heads, Ball Bearing, Stand

2. Prime mover/Dynamometer: that will rotate the NCI samples with a speed of 60 rev/min where the frequency of rotation is (f=1Hz).
3. Open-ended waveguide sensor (MO9062) operating at 24GHz and having a footprint equal to the dimensions of the waveguide opening (1.07 cm x 0.43 cm).
4. OP-AMP amplifier in order to amplify the measured reflection coefficient signal.
5. DC voltage source supplying the op-amp with +/-Vcc and to supply the waveguide sensor with 5 V.
6. Data Acquisition (DAQ) card (NI CB-68LP): it has 68 I/O terminals with 250 KS/s. Our sampling frequency is 500 Hz.

2.3 Digital Filters

2.3.1 Digital Low Pass Filter Design

Low pass filters (LPF) are used to remove high frequency components. It can be designed as an infinite impulse response (IIR) or a finite impulse response (FIR). In this thesis, the main focus will be on the finite impulse response because it can provide a linear phase shift, and it is always stable [13]. Figure 2-4 shows a low pass filter example with its specifications.

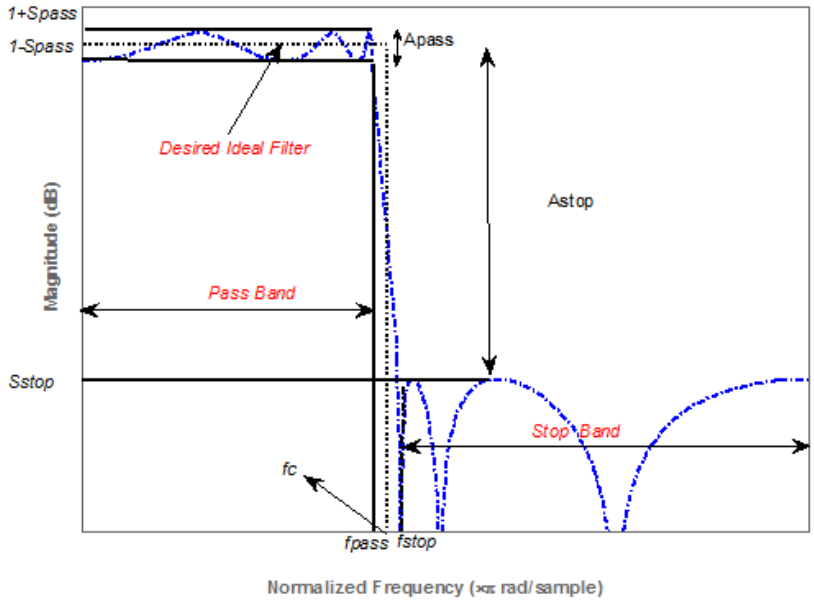

Figure 2-4: Low Pass Filter Design

Windowing method will be used in designing the LPF, where our LPF in the time domain is a windowed Sinc function as shown in equation 2-1[13]:

$$h(n) = W(n)\frac{\mathrm{sinc}(w_c(n-M))}{\pi(n-M)} \qquad (2\text{-}1)$$

Where:

w_c is the cutoff frequency

M: is related to the order of the filter

The Kaiser window was used because of its ability to design filters for any required passing band ripple height (A_{pass}) and stopping band ripple height (A_{stop}),

unlike the hamming and the rectangular windows. After substituting W(n) with its function, equation (2-1) changes to [13]:

$$h(n) = \frac{I_0\left(a\frac{\sqrt{n(2M-n)}}{M}\right)}{I_0(a)} \cdot \frac{\mathrm{sinc}(wc(n-M))}{\pi(n-M)} \quad (2\text{-}2)$$

Where:

I_0: is the Bessel function

The design stage of the LPF includes finding the cut off frequency, the M parameter (which is related to the number of samples of the filter), and the a parameter (which is related to stopping band ripple height). Before starting with the design, some parameters shall be chosen according to the desired specifications of the filter like: the passing band ripple height (A_{pass}), the stopping band ripple height (A_{stop}), the passing frequency (f_{pass}), and the stopping frequency (f_{stop}). Then, other parameters shall be calculated (δ_{pass},δ_{stop}, δ , and A) as given by the equations (2-3)- (2-6) [13].

$$\delta_{pass} = \frac{10^{(\frac{A_{pass}}{fs})}-1}{10^{(\frac{A_{pass}}{fs})}+1} \quad (2\text{-}3)$$

$$\delta_{stop} = 10^{(\frac{-A_{stop}}{fs})} \quad (2\text{-}4)$$

$$\delta = \min(\delta_{pass}, \delta_{stop}) \quad (2\text{-}5)$$

$$A = -20\log_{10}\delta \quad (2\text{-}6)$$

In equation (2-3), fs is defined to be the sampling frequency. After finding all the parameters shown in equations (2-3) - (2-6), the a parameter for the kaiser window is found using equation (2-7)[13].

$$a = 0.112\ (A - 8.7) \quad (2\text{-}7)$$

The next step is to find the cut off frequency, which is defined in equation (2-8)[13]:

$$W_c = \frac{2\pi}{f_s}\ \frac{(f_{pass}+f_{stop})}{2} \quad (2\text{-}8)$$

The last step in the low pass filter design is to find the order of the filter (N) and the M parameters, where the order of the filter shall be rounded up to the next odd integer as given by the equations (2-9) and (2-10) [13].

$$N = 1 + (\frac{Df_s}{\Delta f}) \quad (2\text{-}9)$$

$$M = \frac{1}{2}\,(N-1) \tag{2-10}$$

Where the parameters D and Δf are calculated using equations (2-11) and (2-12).

$$D = \frac{A-7.95}{14.36} \tag{2-10}$$

$$\Delta f = f_{pass} - f_{stop} \tag{2-11}$$

Substituting a, M, and W_c in equation (2-2) will complete the designing stage of our digital low pass filter.

2.3.2 Digital Notch Filter Design

Notch filter is used to remove a single frequency component from the desired frequency range. The main concept behind designing a notch filter is to place a pair of zeros at the same angle of a pair of poles where the pair of zeros has bigger magnitude. The transfer function of the notch filter is given by [13]:

$$H(Z) = \frac{(1-re^{jwo}Z^{-1})(1+re^{jwo}Z^{-1})}{(1-Re^{jwo}Z^{-1})(1+Re^{jwo}Z^{-1})} = \frac{1+b1\,Z^{-1}+b2\,Z^{-2}}{1+a1\,Z^{-1}+a2\,Z^{-2}} \tag{2-12}$$

Where: $b1 = -(2\,r\cos w_0)$, $b2 = r^2$, $a1 = -(2\,R\cos w_0)$, and $a2 = R^2$.

The magnitude response of the notch filter is given by:

$$|H(w)|^2 = \frac{(1-2r\cos(w-w0)+r^2).(1-2r\cos(w+w0)+r^2)}{(1-2R\cos(w-w0)+R^2).(1-2R\cos(w+w0)+R^2)} \tag{2-13}$$

The closer (in magnitude) the pair of poles to the pair of zeros, the narrower the notch width is.

2.4 Feature Extraction

2.4.1 Statistical Features

Statistics serve to estimate model parameters and describe the data. There are several statistical parameters that can be used as features like: mode, median, mean, variance, standard deviation, skewness of the distribution, and kurtosis.

Mode is defined to be the most occurring score value. While the median is the score value that cuts the distribution in half, such that half of these scores fall below the

median and half of theses scores fall above the median. The mean is the sum of the scores divided by the number of them and it can be expressed by [13]:

$$\mu = \frac{\sum_{i=1}^{N} Xi}{N} \quad (2\text{-}14)$$

Where: N is the number of samples, and Xi is the ith data sample.

The variance and the standard deviation are measures of the variability of the data. The standard deviation is the variance squared, where the variance is an indication of the average squared deviation around the mean and it can be expressed as [13]:

$$\sigma^2 = \frac{\sum_{i=1}^{N} (Xi-\mu)^2}{n} \quad (2\text{-}15)$$

Skewness is a measure of lack of symmetry. Usually zero skewness indicates a symmetric distribution. A negative skewness indicates that the left tail is longer than the right tail, while a positive skewness indicates that the right tail is longer than the left tail. skewness is given by equation 2-17 [13]-[15]:

$$Sk = \frac{\sum_{i=1}^{N} (Xi-\mu)^3}{n\,\sigma^3} \quad (2\text{-}16)$$

Kurtosis is a measure of whether the data are peaked or flat near the mean. Data sets with high kurtosis usually have distinct peak near the mean. On the other hand, data sets with low kurtosis values have flat peak near the mean. The kurtosis is given by equation 2-18 [15][16]:

$$K = \frac{\sum_{i=1}^{N} (Xi-\mu)^4}{n\,\sigma^4} \quad (2\text{-}17)$$

2.4.2 Fast Fourier Transform

Discrete Fourier Transform (DFT) is a mathematical procedure used to determine the harmonic, or frequency content of a discrete signal sequence. Radix-2 Fast Fourier Transform (FFT) is a very efficient process for performing DFTs under the constraint that the DFT size to be an integral power of 2 (Number of points in the transform $= 2^k$, where k is a positive integer). FFT reduces the number of complex multiplications from (N^2) to ($\frac{N}{2}\log_2 N$) [13].

In case the bandwidth of the continuous signal is not known, FFT results that have important spectral components near half the sampling may be a big indication of aliasing

(having sampling frequency less than twice the bandwidth of the continuous signal). To solve the aliasing problem, LPF should be applied. This LPF is of cutoff frequency less than half the sampling frequency and more than the range of interest. The number of samples of the digital signal can be chosen according to equation 2-19[13]:

$$N = \frac{fs}{\text{desired frequency resolution}} \quad (2\text{-}18)$$

The N-point FFT can be calculated using the equation 2-20:

$$x(m) = \sum_{n=0}^{\frac{N}{2}-1}(X(2n)\, W_{\frac{N}{2}}^{nm}) + W_N^{nm} \sum_{n=0}^{\frac{N}{2}-1}(X(2n+1)\, W_{\frac{N}{2}}^{nm}) \quad (2\text{-}19)$$

Where m=0, 1, 2 ...N-1 and $W_N^{nm} = e^{-j\pi(nm)/N}$

2.4.3 Wavelet Transform Analysis

Short time frequency transform (STFT) is a time- frequency representation of a certain signal. Choosing the window size in STFT is one of the most challenging issues, because choosing a small window size will achieve good time resolution and bad frequency resolution. On the contrary, choosing a big window size will give a bad time resolution and a good frequency resolution. Wavelet transform is a multi-resolution analysis, where the problem of deciding the window size doesn't appear in wavelet analysis. At low frequency bands, the wavelet transform has good frequency resolution and bad time resolution, and the opposite at high frequency bands [17][18]. Discrete Wavelet Transform (DWT) can be expressed as[17]:

$$W(j,K) = \sum_{n=0}^{N-1} f(n).\varphi_{j,k}(n)^* \quad (2\text{-}20)$$

Where:

W (j, K) is DWT coefficient

f(n) is the digital signal that DWT is performed on.

The discrete wavelet basis is defined to be:

$$\varphi_{j,k} = \frac{1}{\sqrt{S_0^j}}\, \varphi\left(\frac{n - S_0^j.K}{S_0^j}\right) \quad (2\text{-}21)$$

(S_0^j) and ($S_0^j.K$) are defined to be the discrete version of the scale and translation parameters[18].

Practically, the wavelet basis corresponds to high pass and low pass filters in a filter bank. The output of the high pass filter is called the first detail coefficients of DWT and the LPF output is called the first approximation coefficients. The first approximation is down sampled by a factor of 2 and passed in to a new low pass and high pass filter to generate another DWT detail and so on [17][18]. The mother wavelet used is the symlet where the high- pass and low pass decomposition filters used are illustrated in Figure 2-5.

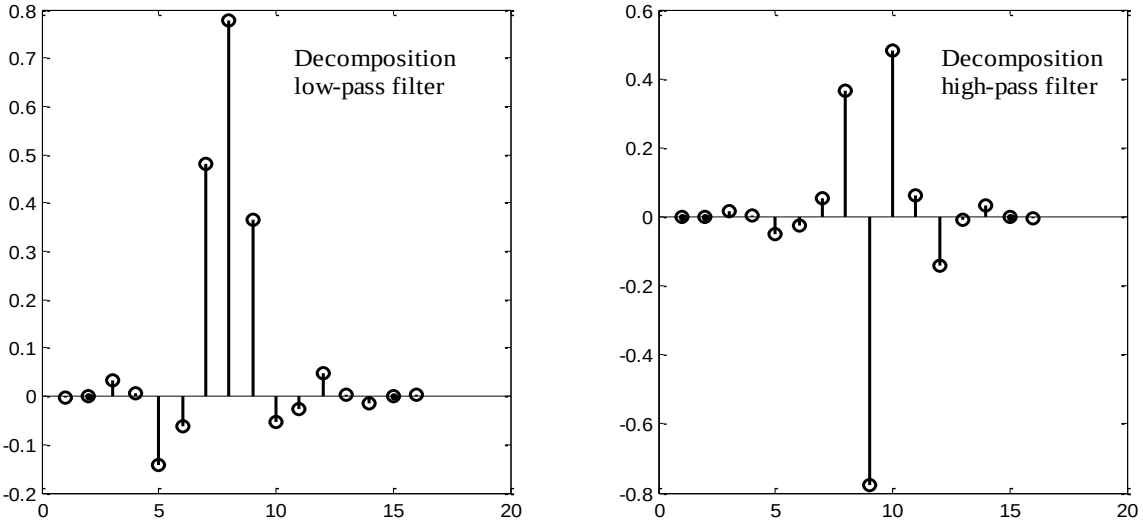

Figure 2-5: Filters used for wavelet decomposition

The details and approximation can be found by equations 2-23 and 2-24:

$$D_{j+1}(i) = \sum_{L=0}^{l-1} HPF(L).A_j(2.i + L) \quad (2\text{-}22)$$

$$A_{j+1}(i) = \sum_{L=0}^{l-1} LPF(L).A_j(2.i + L) \quad (2\text{-}23)$$

In this work, the energy of the 4-details wavelet decomposition is used as extracted features. Figure 2-6 illustrates the block diagram of the wavelet transform methodology [17].

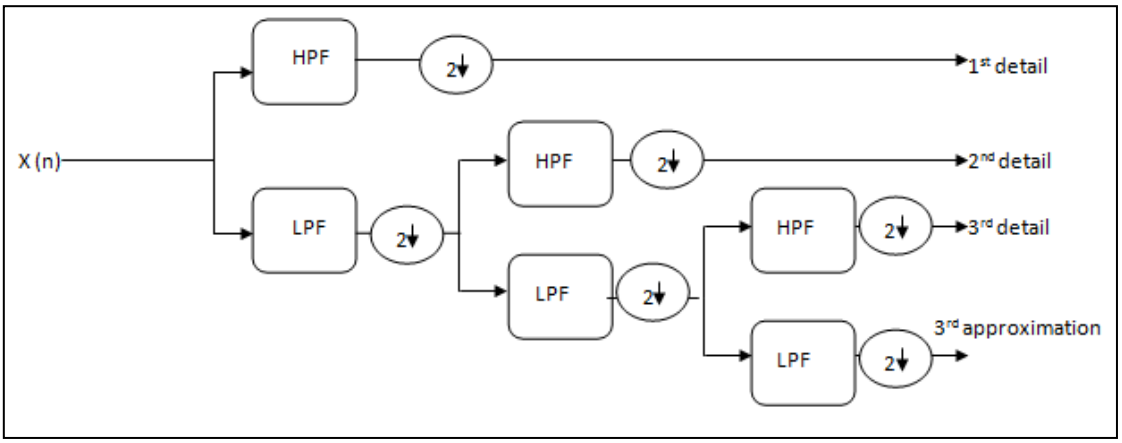

Figure 2-6: block diagram of Discrete Wavelet Transform

2.5 Step-wise Regression

Stepwise is used as a feature extraction technique based on the statistical significance of the features. It is of great importance when having redundant input features that are confusing the classification process.

Assume having K input features (X1, X2, … Xk), one intercept $\beta 0$, and a single response variable y corresponding to the class label. The stepwise regression procedure is summarized as following [19][20]:

1. It starts by building a one variable regression model using the variable that has the highest correlation with the response variable y. Moreover, this variable has the highest partial F-statistic.
2. The remaining K-1 variables are tested by comparing their F-statistic with the F-random variable for adding variables (f_{in}). The feature with the highest partial F-statistic value, given that the F-statistic of that feature is more than (f_{in}), is included in the model. The F-statistic can be calculated by equation 2-24 :

$$F_j = SS_R(\beta_j | \beta_0, \beta_1, \dots\dots\dots, \beta_{j-1}, \beta_{j+1}, \dots., \beta_k)/MS_E \quad (2\text{-}24)$$

$$SS_R = \sum_{n=1}^{N}(\hat{Y} - \overline{Y})^2 \quad (2\text{-}25)$$

Where:

β_j: is The regression coefficient due to adding Xj to the model.

$\beta_{j-1}, \beta_{j+1}, \dots., \beta_k$: are the regression coefficients for the terms that are currently in the model.

MS_E: corresponds for the mean square error for the model.

$SS_R(\beta_j | \beta_0, \beta_1, \dots\dots\dots, \beta_{j-1}, \beta_{j+1}, \dots., \beta_k)$: indicates the regression sum of squares due to β_j given that $\beta_0, \beta_1, \dots\dots, \beta_{j-1}, \beta_{j+1}, \dots., \beta_k$ are already in the model.

$\hat{Y}$: is the presicted variable (Class Label).

N: is the number of observations (measured signals).

$\overline{Y}$: is the mean of all observations.

3. If variable X2 is added to the model, the procedure determines whether variable X1 shall be removed from the model or not. At this stage, the partial F-statistic of all previously added random variables are compared with the F-random variable of removing variables from the model (f_{out}) and accordingly a decision is taken on keeping or removing that variable.
4. The same procedure is done for all remaining variables where the decision of stopping is taken when no other variables can be added or removed from the model.

In this work, the stepwise regression is used in order to extract the important features according to their statistical significance. This will result in successful classification of different defects in outdoor insulators. Matlab is used as a feature modeling environment where terms are added or removed according to the F-statistic value [16].

Some of the statistical parameters used for comparing the different regressive models are F-statistic, adjusted R^2-statistic, and root mean square error. The F-statistic is a measure of the statistical significance of certain variable. In addition to that, it is an indication of the correlation between certain feature and the predicted variable. The R^2-statistic measures the variation of the predicted variable (class label) with respect to the

selected feature in a model. When R^2-statistic=1, it represents best fit between the features and predicted variable. The R^2-statistic is given by [19] [20]:

$$R^2 = 1 - \frac{SSE}{SST} \quad (2\text{-}26)$$

Where SSE is the sum of square error, and SST is the sum of square total. They are both given by equations 2-28 and 2-29:

$$SSE = \sum_{n=1}^{N} \left(Y - \hat{Y}\right)^2 \quad (2\text{-}27)$$

$$SST = \sum_{n=1}^{N} (Y - \overline{Y})^2 \quad (2\text{-}28)$$

R^2-statistc depends on the number of the predicted variables in the fitted model. That's why adjusted R^2-statistc is used in comparing between different models with different number of input variables. Adjusted R^2-statistc is given by equation 2-30:

$$\text{adj.}\, R^2 - \text{stat.} = 1 - \frac{(1-R^2)(n-1)}{n-p-1} \quad (2\text{-}29)$$

Where, P is defined to be the number of input variables in each model (number of features).

2.6 Artificial Neural Networks (ANN)

Neural Network is a multi-layer network that maps input in to a certain output. Figure 2-7 shows the structure of the neural network that was used in this thesis.

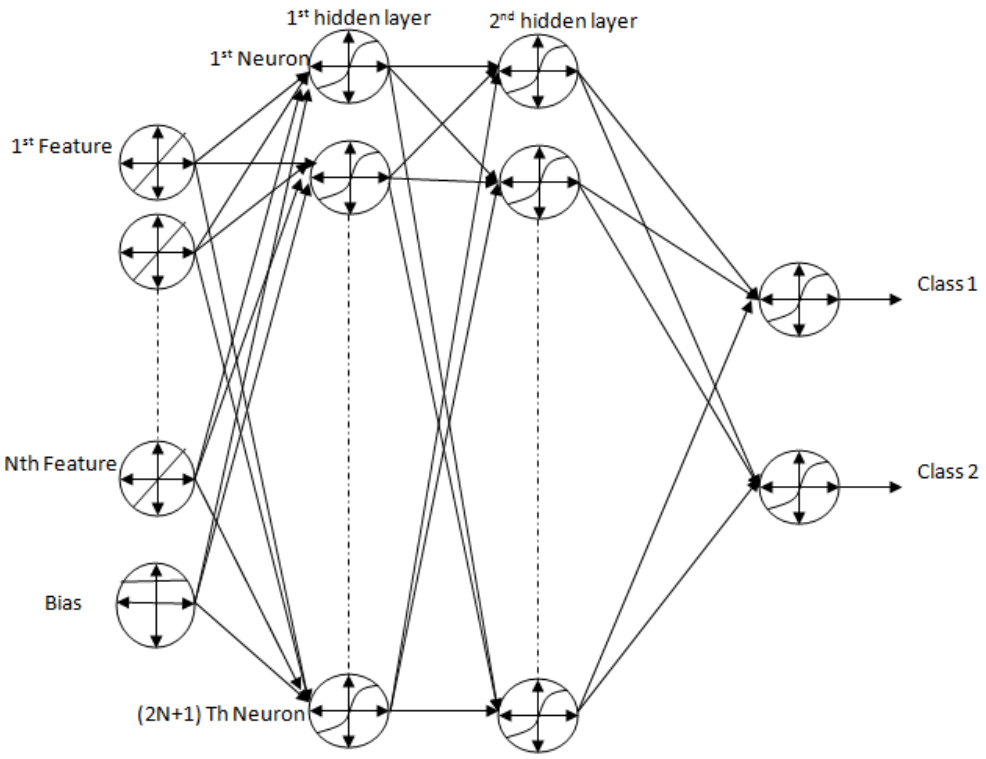

Figure 2-7: Multilayer- Perceptrons Neural Network

In this thesis, four neural networks were used. The purposes of theses neural networks are detecting the defect in silicone rubber layer, specifying the defect type in the silicone rubber layer (metal, or air void), detecting the defect in the reinforced fiberglass core, and specifying the defect type in the fiberglass core (crack or air void). Figure 2-7 shows the structure for all neural networks used. The structure includes an input layer, two hidden layers, and an output layer. The output of j^{th} hidden unit in the first hidden layer is given by:

$$y_j = f(netj) = f(\sum_{i=1}^{d} (w_{ji}x_i + w_{j0})) \quad (2\text{-}30)$$

Where:

y_j Indicates the output of the j^{th} hidden unit in the first hidden unit

w_{ij} Indicates the weights between the i^{th} input and the jth neuron

w_{jo} Indicates the weights between the bias and the jth neuron

$\sum_{i=1}^{d}(w_{ji}x_i + w_{j0})$ is called the activation and f (netj) is the non linear function of the activation (activation function)

The output of (L^{th}) hidden unit in the second hidden layer is given by:

$$F_L = f(\sum_{j=1}^{Nm}(w_{Lj}y_j + w_{L0})) \quad (2\text{-}31)$$

Where:

F_L indicates the output of the Lth hidden unit in the second hidden layer.

w_{Lj} indicates the weights between the Lth neuron in the second hidden layer and the jth neuron in the first hidden layer.

Nm is the number of neurons in the first hidden layer.

The output of the neural network can be represented by [21]:

$$Z_k = f(\sum_{L=1}^{n_H}(w_{kL}F_L + w_{k0}))$$

(2-32)

Where n_H is the number of hidden units in the second layer.

There is no specific rule or equation that helps finding the activation function. But in general, the activation should be chosen such that it is continuous, smooth, differentiable, non-linear (so that it doesn't operate as a 2-layer network), and saturates after a certain value in order to keep the weights bounded and consequently the training time [21]. In this thesis, the tan sigmoid function is used as the activation function for all neurons.

2.6.1 Training ANNs

Before using the neural network in the feed forward operation for testing purpose, it shall be trained using enough number of samples. Back propagation algorithm is a supervised training method that finds the effective error by each hidden layer. In supervised learning, the weights are updated in each epoch in order to reduce the calculated error. The error is defined in equation 2-34:

$$J(w) = \frac{1}{n}\sum_{k=1}^{c}(T_k - Z_k)^2 \quad (2\text{-}34)$$

T, Z, and C are defined to be the target output, actual output, and length of output vector respectively. In each epoch, the weights are updated using gradient descent (Δw) of the error surface and a chosen learning rate as shown in equation 2-35:

$$w(m+1) = w(m) + \Delta w \quad (2\text{-}35)$$

Where the gradient descent of the error surface is: $\Delta w_{pq} = -\eta dJ/dw_{pq}$ and η is the learning rate which will define the step size of our learning process.

In large step size, the converging state can be approached quicker. On the other hand, very long step size may overstep the solution and go off in the wrong direction. Small step size will go in the correct direction but may need a very large number of epochs to achieve convergence.

Table 1 shows the number of epochs and the mean square error for each neural network used. The stopping criterion is reaching a zero mean square error.

Table 1: Number of epochs and the mean square error for the ANNs proposed

Purpose of the ANN	Number of Epochs	Mean Square Error
Detect defects in the silicone rubber layer.	17	0.0479
Specify the defect type in the silicone rubber (air void, or metal inclusion)	50	$4.6x10^{-12}$
Detect defects in the fiberglass core.	15	0.0245
Specify the defect type in the fiberglass core (crack, or air void)	40	$1x10^{-11}$

In order to ensure that the testing samples are not biased to give high classification rates, swapping between some of the training samples and testing samples was done. This process was done 20 times where the classification rate that is mentioned in the results chapter is the average of the classification rates.

CHAPTER 3: Results and Discussion

3.1 Electric Field Calculation

Before starting with the near-field microwave non destructive testing, it is important to show the deficiency of other testing techniques. Insulation resistance measurement, partial discharge test, and electric field measurement are testing techniques that are correlated with the electric field distribution. So, the results of electric field calculations are done by finite element method (FEM) software called COMSOL where two types of defects are simulated (air voids, and conductive inclusions). The shape and the size of the COMSOL simulated defects match the actual defects created in the laboratory. Figure 3-1 shows the electric potential distribution on the simulated non ceramic insulator (NCI).

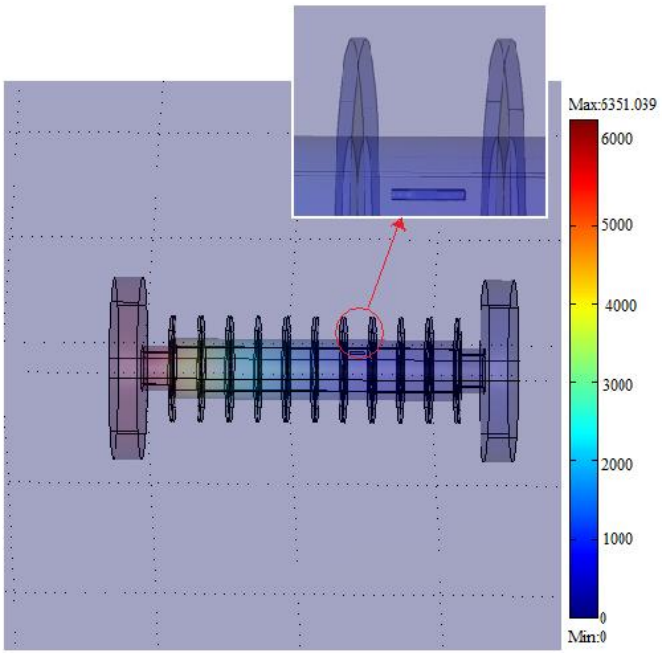

Figure 3-1: 3-D simulation of defected NCI using COMSOL software

After that the electric field 1mm away from the NCI surface is calculated using COMSOL software. The results obtained for different sizes of defects (air voids and metal inclusions) are shown in Figure 3-2.

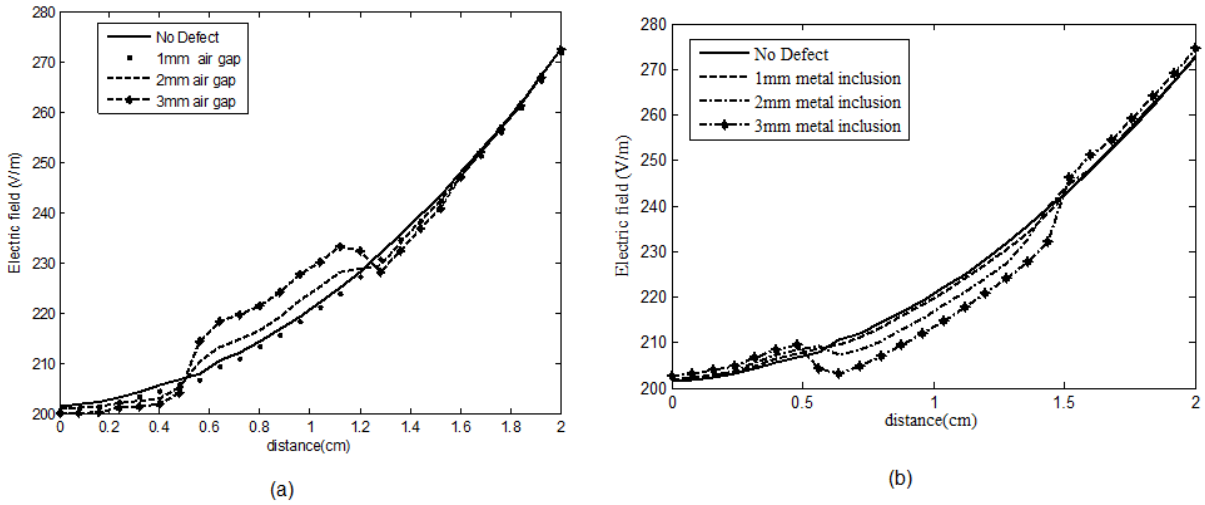

Figure 3-2: (a) Electric field profile for air voids with different sizes (b) Electric field profile for metal inclusion with different sizes

As can be noticed in Figure 3-2, unless the defect radius is really big (3mm), it is not creating a noticeable electric field difference. It can be concluded from the results in Figure 3-2 that the electric field based methods are not dependable techniques to detect defects. Moreover, electric field based techniques requires energizing the insulator.

3.2 Signal Acquired from Near-field Microwave Sensor

3.2.1 Signals Acquired for the Silicone Rubber Defects

In this section, the signals acquired from the near microwave experimental setup are presented. This technique has showed very high sensitivity to any change in the permittivity of the dielectric material. Some signals show clear difference between defected and non defected samples as demonstrated in Figure 3-3.

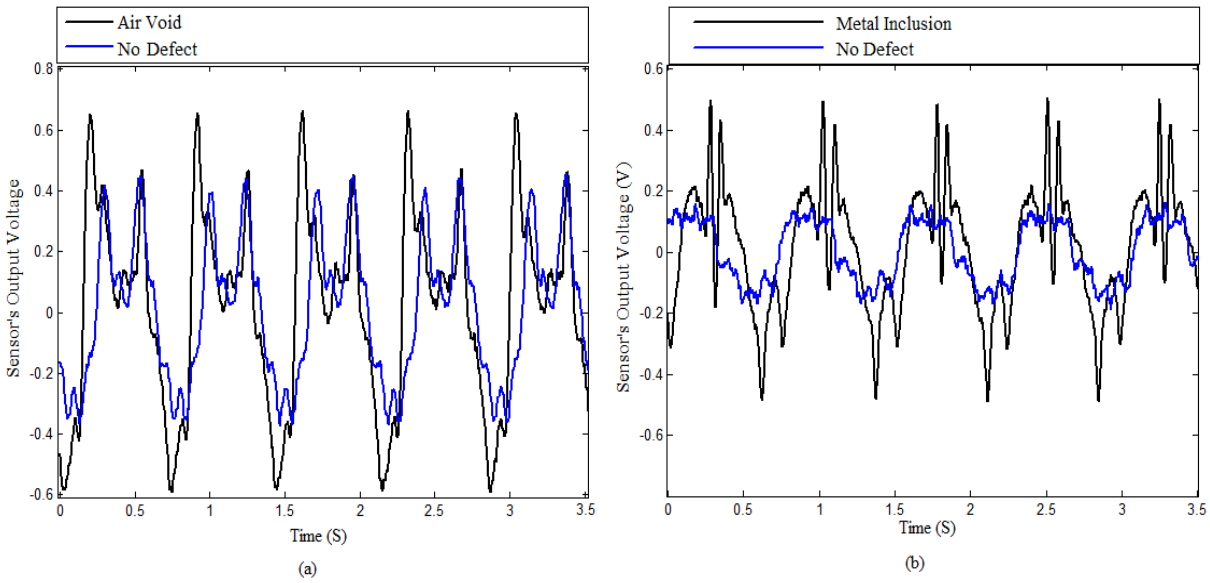

Figure 3-3: (a) The signal of the Air Void defect compared with the No defect signal (b) The signal of Metal inclusion defect compared with the No defect signal

The frequency responses of the signals given in Figure 3-3 are illustrated in Figure 3-4.

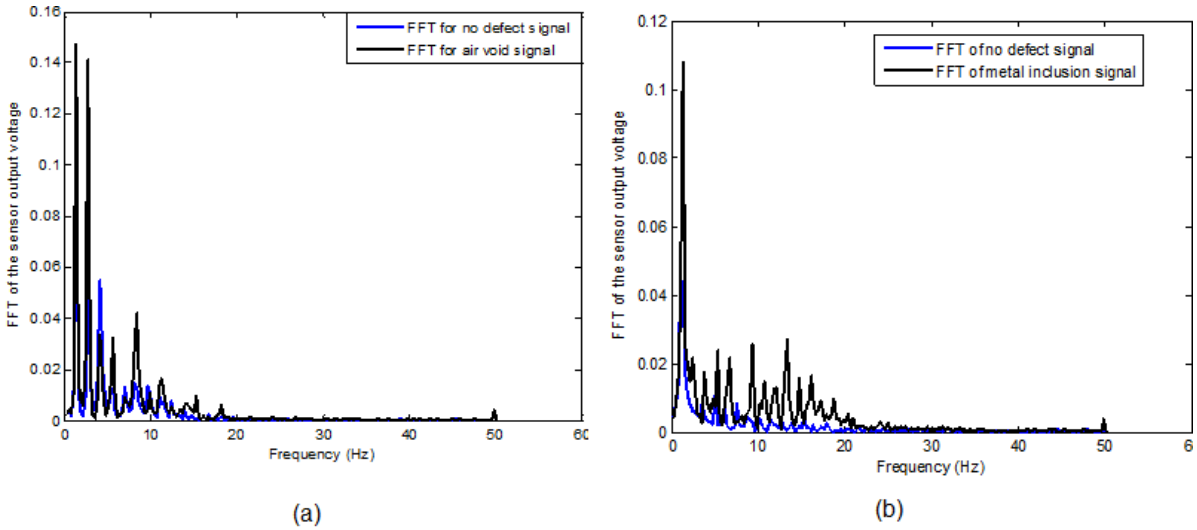

Figure 3-4: (a) FFT of air void signal compared with FFT of no defect signal, (b) FFT of metal inclusion signal compared with FFT of no defect signal

On the other hand, there are some cases where differentiating between defected and non defected samples is a very hard task using near-field microwave NDT. This can be depicted in Figure 3-5.

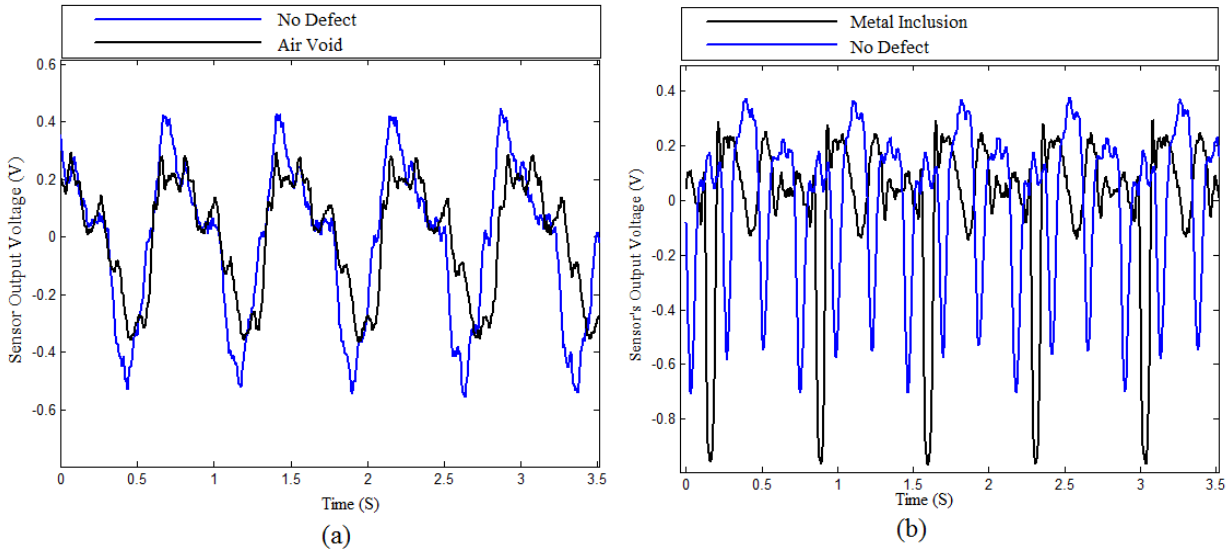

Figure 3-5: (a) The signal of the Air Void defect compared with the No defect signal (b) The signal of Metal inclusion defect compared with the No defect signal

The FFT of the signals in Figure 3-5 are described in Figure 3-6.

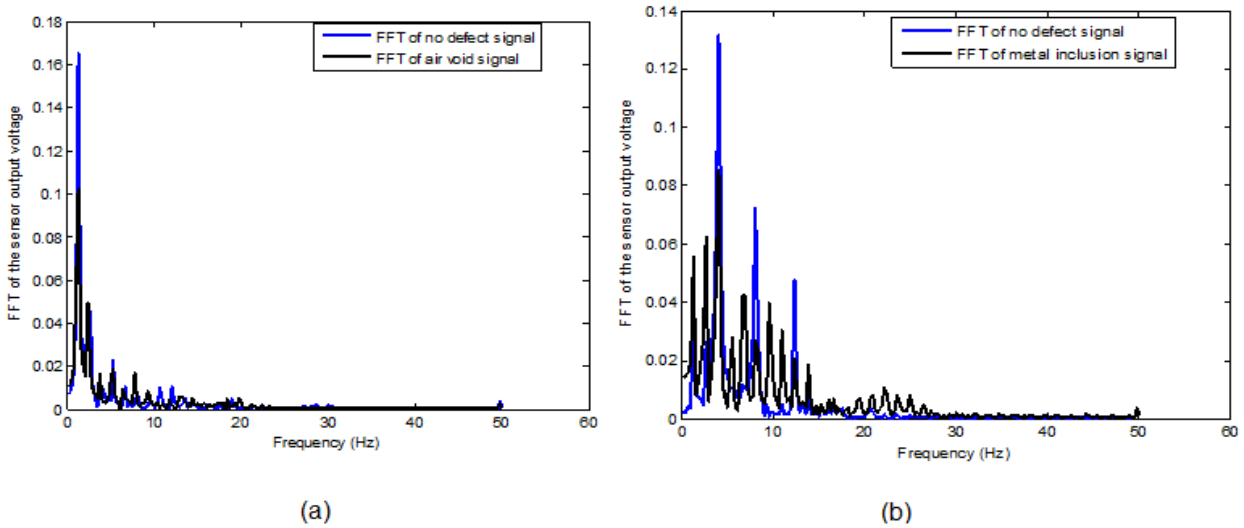

Figure 3-6: (a) FFT of air void signal compared with FFT of no defect signal, (b) FFT of metal inclusion signal compared with FFT of no defect signal

Although it can be noticed that the important frequency range is (0-50Hz), Figure 3-4 and Figure 3-6 show that it is not easy to find the exact differentiating frequency components between defected and none defected samples. In addition to that, an automated system is needed in order to approach a reliable detection technique. Thus, signal processing and artificial intelligent tools are utilized in this testing method.

3.2.2 Signals Acquired for the Fibreglass Core

Similar to the silicone rubber case, the microwave sensor's signal of a fibreglass core is acquired. Figure 3-7 compares between the signals of defected fibreglass core (air void and crack) and the no defect signals.

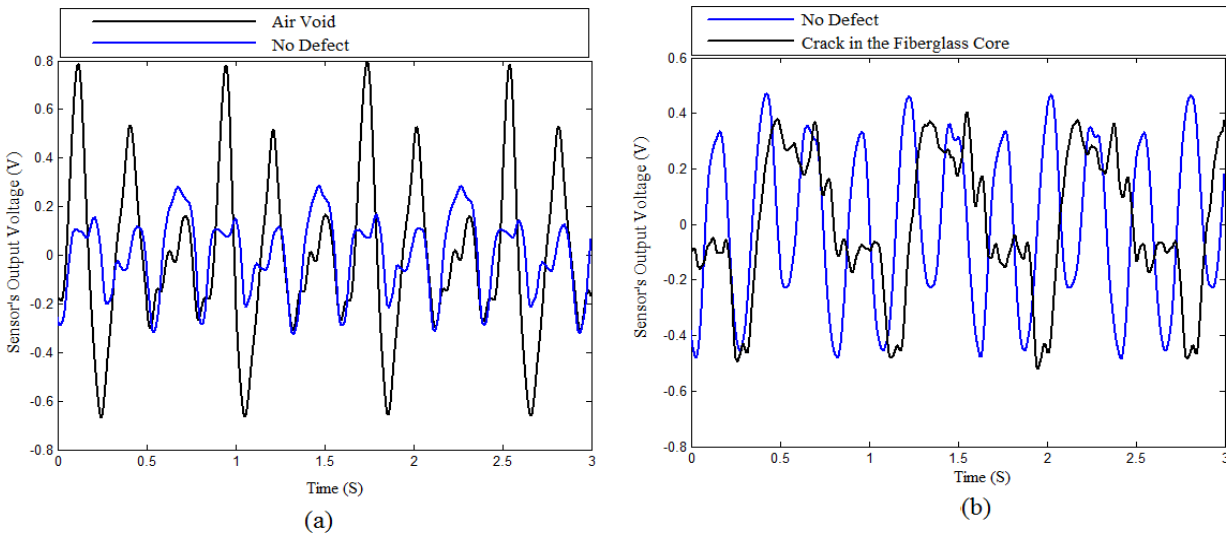

Figure 3-7: (a) The signal of an air void in the fiberglass core compared with no defect signal (b) The signal of cracked fiberglass core compared with no defect core

The frequency responses of the signals shown in Figure 3-7 are represented in Figure 3-8.

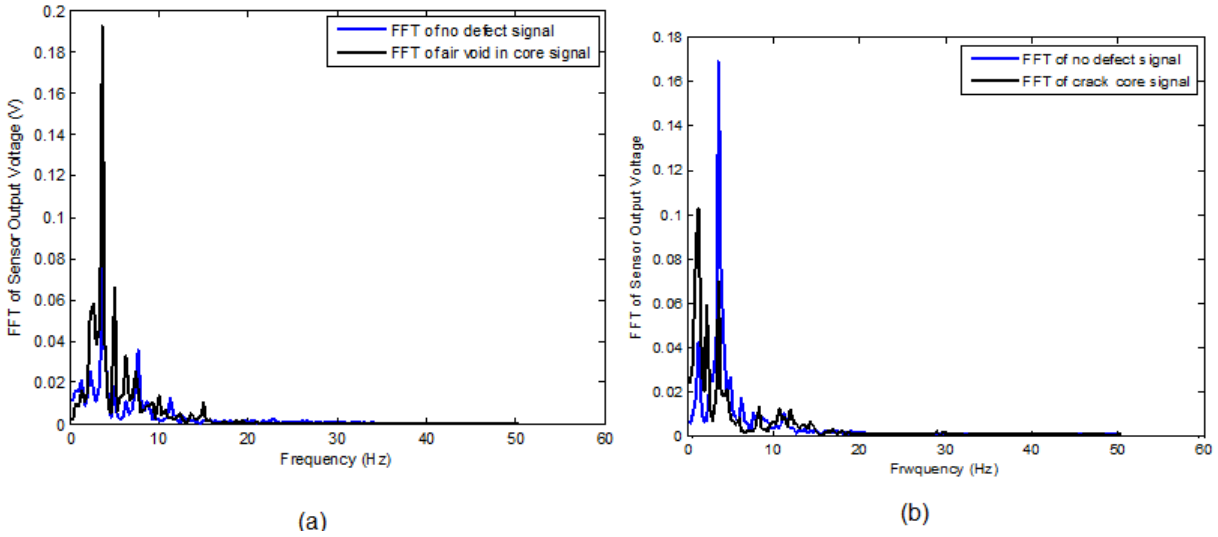

Figure 3-8: (a) FFT of an air void signal in the fiberglass core compared with FFT of no defect core signal(b) FFT of cracked fiberglass core signal compared with FFT of no defect core signal

Unlike the silicone rubber case, Figure 3-8 shows that the important frequency components are in the range (0-20) Hz.

3.3 Digital Filters

In order to explain the importance of the filtering process, the air void signal shown in Figure 3-9 will be taken as an example.

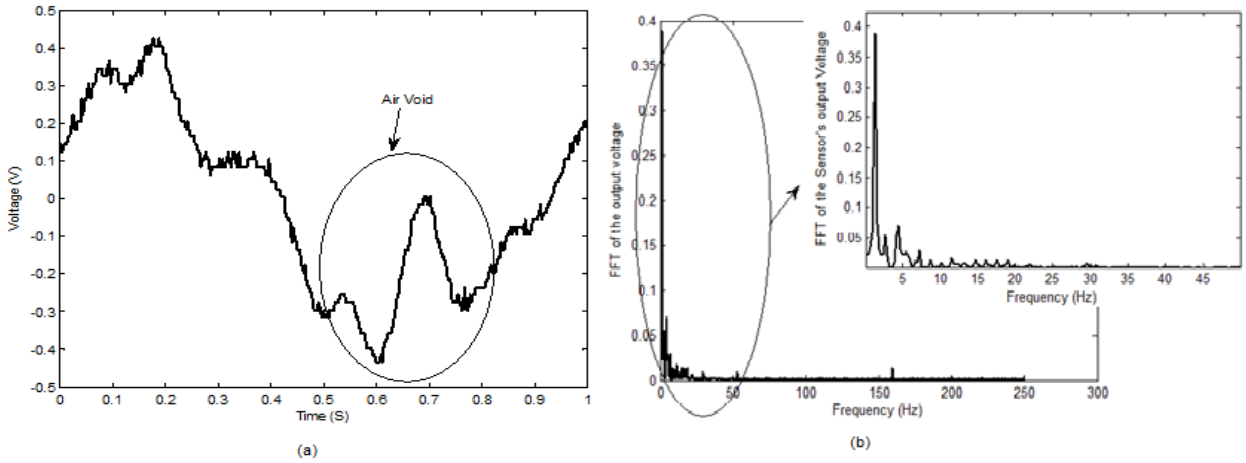

Figure 3-9: (a) Signal of an Air Void in the silicone rubber (b) Fourier Transform the air void signal

Figure 3-9 contains information about the air void plus some noise. The location of the air void in the signal was identified because its physical location in the insulator is known to us. It was noticed that the acquired signal has a relatively strong 1 Hz frequency component when the NCI is rotated with a 60 Rev/min speed. This frequency component is due to the cyclic effect of the variation of thickness in the silicone rubber layer [7]. In addition to that, it was found that the acquired signals have noise at all frequency components above 50 Hz. In order to remove these frequency components, a low pass filter is used. Our designed low pass filter has a passing frequency of (f_{pass} = 50 Hz), a stopping frequency (f_{stop} = 60 Hz), ($\delta_{pass} = 0.01$), and ($\delta_{stop} = 0.05$). The magnitude frequency response of this LPF is demonstrated in Figure 3-10.

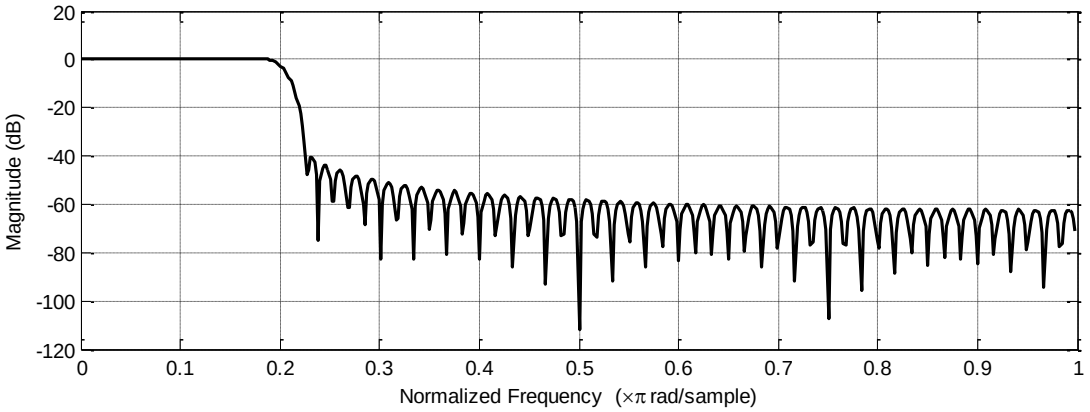

Figure 3-10: Magnitude response of the designed LPF

The signal after applying the designed low pass filter is shown in Figure 3-11.

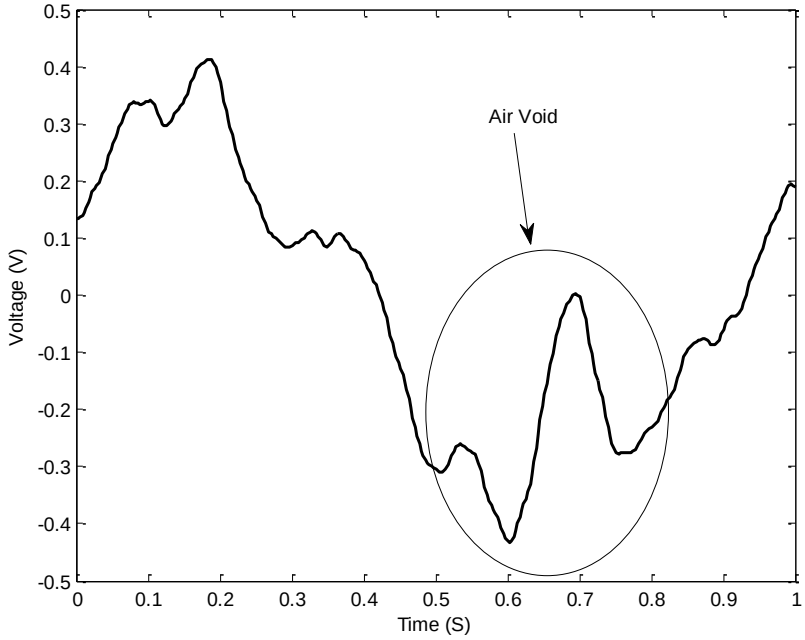

Figure 3-11: The signal of an air void in the silicone rubber layer after applying LPF to it

After that, the cyclic effect of the silicone rubber thickness variation is removed using a notch filter. The cut off frequency of this notch filter is 1 Hz, where its magnitude response is shown in Figure 3-12.

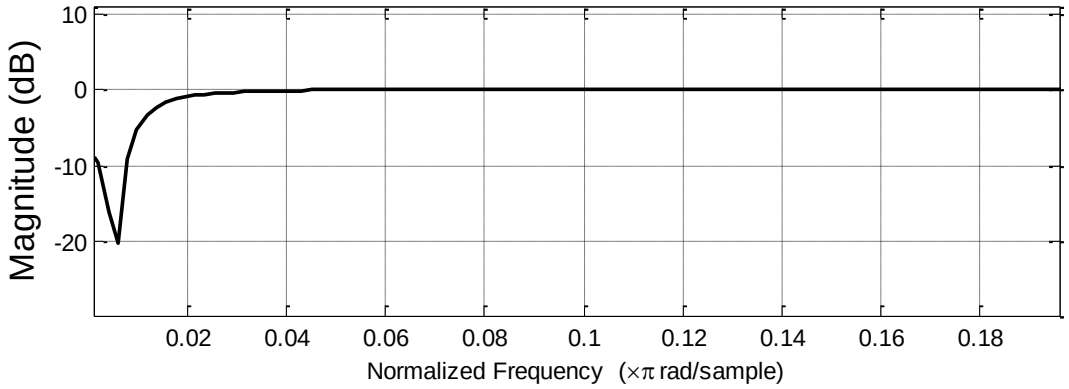

Figure 3-12: Magnitude response of the designed notch filter

Figure 3-13 shows the signal after applying the notch filter where the effect of the air void is emphasized. As can be noticed, the signal still contains noise. This noise is due to the vibration of the mechanical system and the molding line in the silicone rubber layer. Moreover, the difference in permittivity between the filler material and the fiberglass material in the core is also contributing in noising the sensor's output voltage. This type of noise is very hard to remove since its frequency is overlapping with important frequency components.

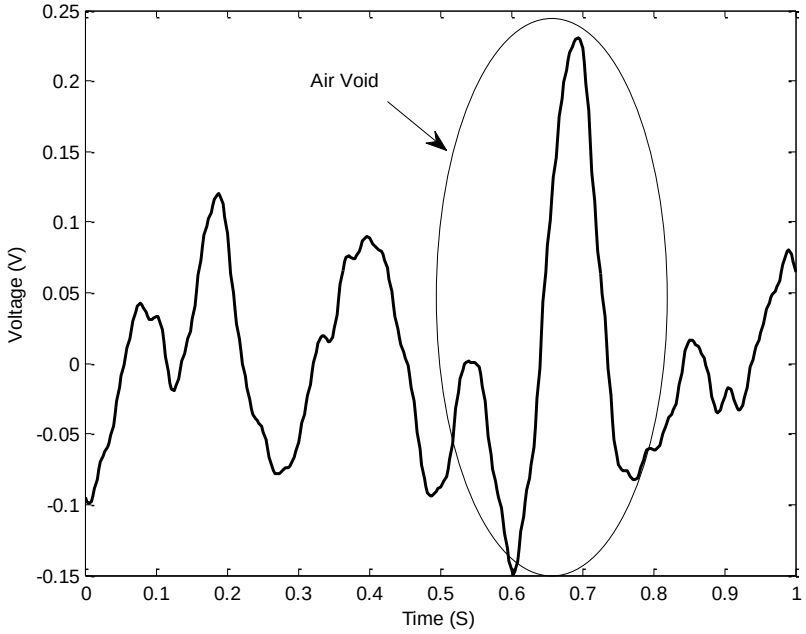

Figure 3-13: Filtered air void signal

For the signals acquired from the fiberglass core, the silicone rubber layer doesn't exist. As a result, there is no need to use the notch filter and only the low pass filter is applied.

3.4 Wavelet Transform

In addition to the statistical features and FFT components, energy of wavelet details is used as features that may help in the classification process. In some cases the 4-detail wavelet decomposition shows a potential to differentiate between the defected and non defected samples. Before performing wavelet decomposition, the signals are exposed to normalization, low pass filtering, and down sampling by a factor of 4. Figure 3-14 shows a metal included NCI signal and no defect NCI signal.

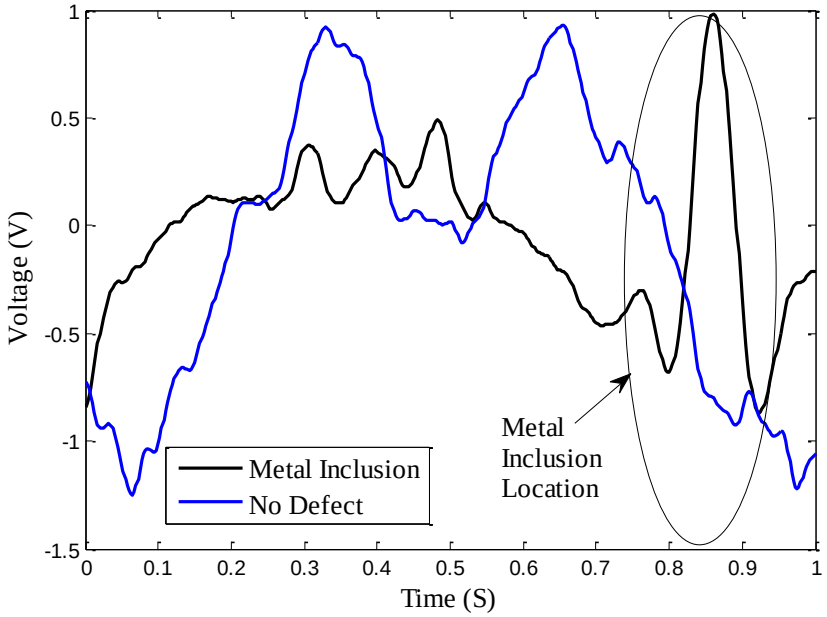

Figure 3-14: metal inclusion signal compared with no defect signal

The signal is decomposed into four details, where each detail corresponds to the time representation of a certain frequency band as represented in Figure 3-15.

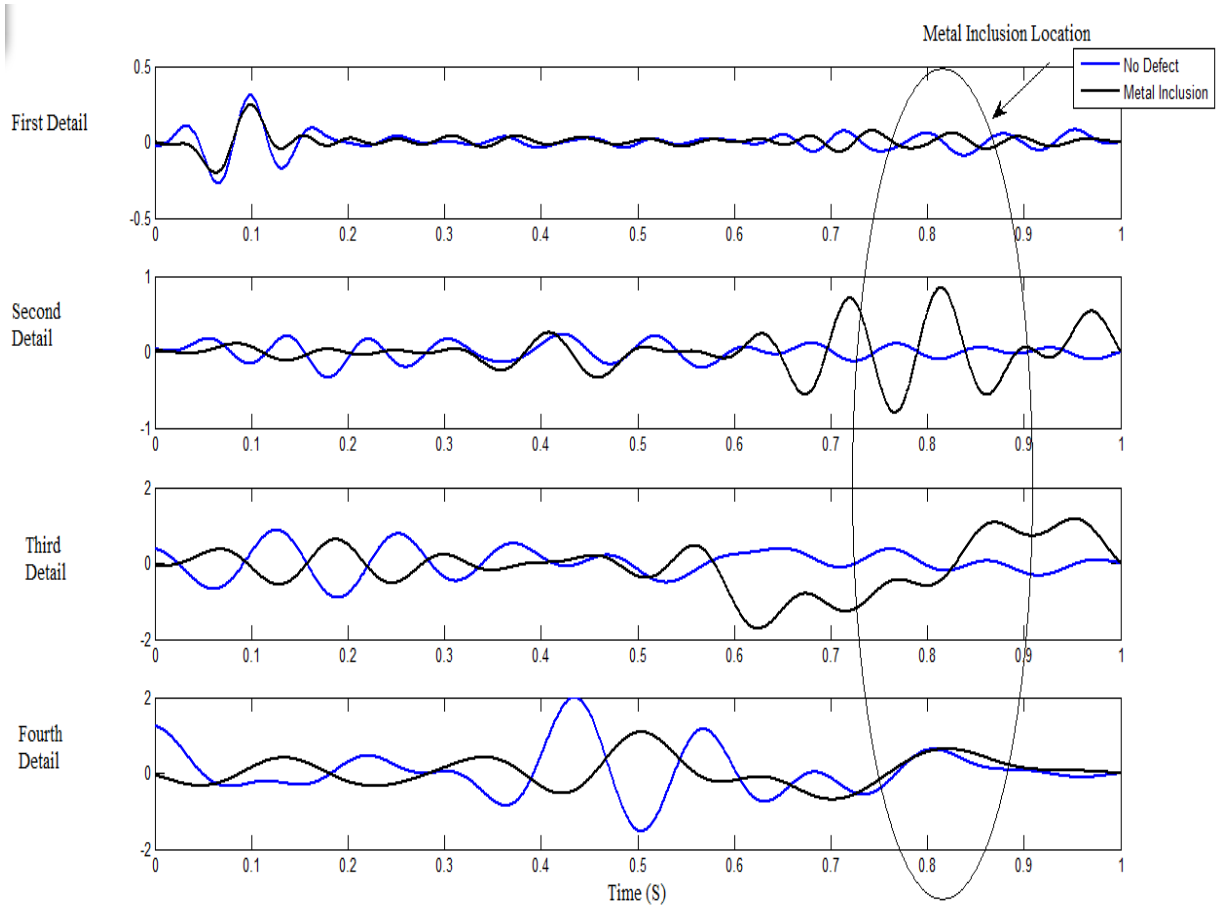

Figure 3-15: 4-detail wavelet decomposition of metal inclusion signal and no defect signal

Figure 3-15 shows that the second detail contains important information about the metal inclusion. The effect of metal inclusion is not perfectly clear, because the vibration of the mechanical system and the molding line noise are of very close frequency band to the defect's frequency band. In some cases, the defect is not clear in the details of the wavelet decomposition. Figure 3-16 shows the time signal of an air void and a no defect NCI samples.

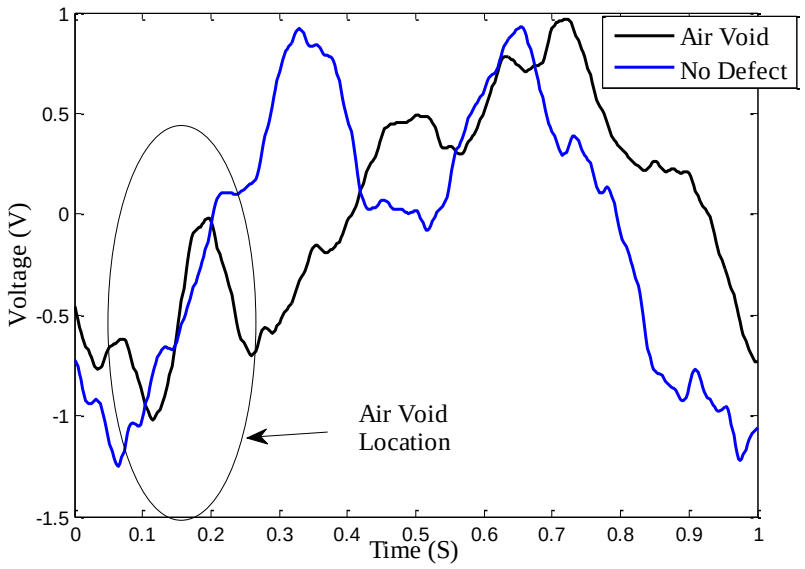

Figure 3-16: Air void compared with no defect signal

Figure 3-17 illustrates the 4-detail wavelet decomposition of the signals shown in Figure 3-16, where the air void's effect is not as clear as the metal inclusion's effect. This is because of the high imaginary permittivity of the metal which can be noticed in the time domain signal.

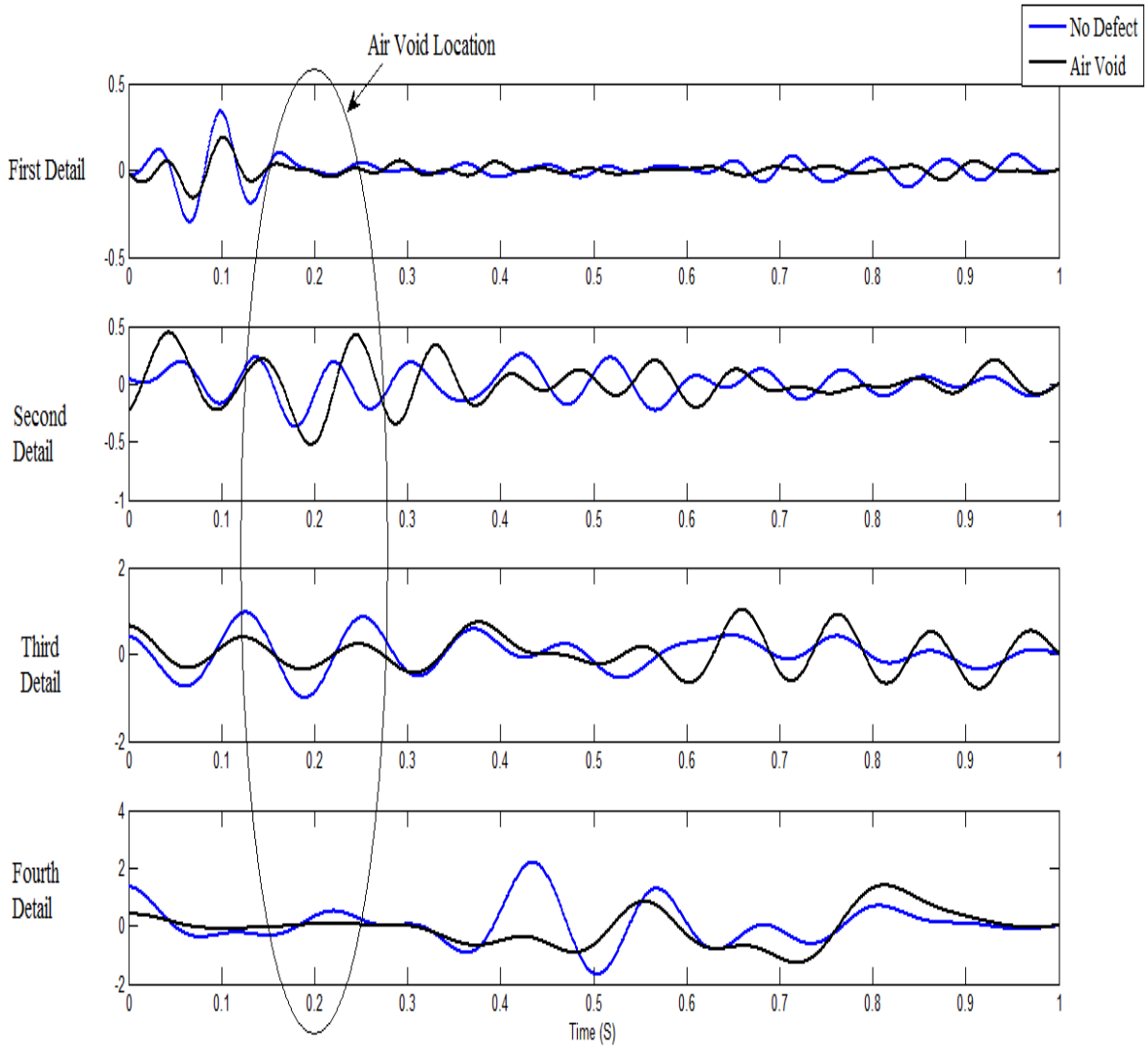

Figure 3-17: 4- detail wavelet decomposition of an air void signal and no defect signal

3.5 Model Input Features

3.5.1 Input Features for Silicone Rubber Layer Defects

This part is divided in to two stages. The first stage includes finding input features that will help classification between defected and not defected insulator samples. In the second stage, our aim is to find the necessary features for the classification between different types of defects in the silicone rubber layer, i.e. air void and the metal inclusion.

After normalizing the filtered signals, stepwise regression is the tool used for removing redundant features. The frequency components, statistical features, and energy of four details wavelet analysis are the input features that need to be reduced. Different initial terms give different models. As a result, a comparison between these different models is done according to the statistical significance of the terms included in these models. Two of the highest statistically significant models that are used in classifying defected and none defected samples are shown in Table 2. Moreover, Table 3 demonstrates two of the best models that can be used in identifying the type of defect in the silicone rubber layer, i.e. air void or metal inclusion.

Table 2: Different models used in classification between defected and non defected insulators

Model Inputs(Features)	Adjusted R-square	F-statistic
The variance, and the frequency components at (8.1, 8.4, 13, 17.8, 23.8, 25, 30.4, 39.2, 43.5, 44.7) Hz.	0.8	24.5
Frequency components at (8.4, 13, 18, 23.8, 25, 30.4, 39.2, 43.5) Hz.	0.75	20.3

Table 3: Different models used in classification between air void and metal inclusion defects

Model Inputs(Features)	Adjusted R-square	F-statistic
The frequency components at (18.7, 19.2, 20.7, 24.4, 39.2, 43.5, 44.6, 47.8) Hz	0.75	40.4
Variance, and the frequency components at (19.2, 24.4, 25.3, 39.2, 43.5, 44.6, 47.8) Hz	0.72	30.5

The terms in the first model in both Table 2 and Table 3 have more statistical significance than the terms in the second model and that is obviously noticed from the adjusted R-square and F-statistic values. The defected case can either be an air void or a metal. The metal inclusion signal has an abrupt and strong change effect on the output voltage of the near filed microwave sensor as noticed in Figure 3-3. On the other hand,

the air void has less change effect on the sensor's output voltage as also noticed in Figure 3-3. As a result, it is only reasonable to expect that the important frequency components are spread all over (0-50 Hz) frequency spectrum and not concentrated in more specific range. Moreover, a measure of how the data are far from the mean is also expected to have a major significance. Hence, Table 3 shows that the variance is one of the features included in the first model.

3.5.2 Input Features for Fibreglass Core Defects

The same initial features used in the case of the silicone rubber are used in starting the stepwise regression model for the fibreglass cases. It is important to mention that the feature extraction process is done after normalizing all the filtered signals. This part aims to classify between defected fibreglass core and non defected core. Additionally, it targets to identify the type of defect, i.e. air void or crack. By varying the initial terms, different models were analyzed and only two were chosen according to their statistical significance as shown in Table 4 and Table 5.

Table 4: Different models used in classification between defected and non defected fiberglass core

Model Inputs(Features)	Adjusted R-square	F-statistic
Frequency Components at (2, 2.5, 3.25, 3.75, 4.25, 5.25,7,10,17.5, 17.75,20) Hz	0.95	30.5
Frequency Components at (3.25, 3.9, 4.1 4.25, 5.25,7.2,18.5, 19.2, 21.3) Hz	0.85	25.5

Table 5: Different models used in classification between air void and Crack defects in fiberglass core

Model Inputs(Features)	Adjusted R-square	F-statistic
Frequency Components at (2.75, 4.25, 6, 7.24, 7.5, 7.75, 9.25, 9.5, 12.498)	0.816	36
Frequency Components at (2.1, 2.75, 4.25, 6, 7.24, 9.25, 9.5, 15)	0.75	27.5

Unlike the silicone rubber layer cases, the statistical features of fibreglass core signals did not show any significance. This is may be due to the noise coming from the different permittivity between the filler material and the fibre material. Moreover, the Fourier Transform analysis shown in Figure 3-8 indicated that the discriminating frequency components are concentrated in the (0-20) Hz band. The results shown in Table 4 and Table 5 confirms with our observation.

3.6 Classification Using ANN

3.6.1 Classification for Silicone Rubber Layer Defects

This part includes two artificial neural networks (ANN) with two different purposes and both are related to defects in silicone rubber layer. In the first ANN our aim is to classify between defected and non defected insulators as shown in Table 6. In the second ANN, the goal is to specify the type of defects whether it is an air void or a metal inclusion as explained in Table 7.

Forty signals from each class were acquired. Half of these signals are used for testing and the other half is used for training. At the beginning, ANN was applied on all the extracted features (frequency components, energy of the details found from the 4-detail wavelet analysis, and statistical features). Then, ANN was applied on some feature models including the models found in Table 2 and Table 3.

Table 6: The results of ANN used for classifying defected and non defected NCIs

Feature Vector	Total Number of Testing samples (20 non defected, 20 defected)	Average Classification Rate
Statistical Features	40	52.50%
Frequency Components (0-50 Hz)	40	70.0%
4- details Wavelet	40	62.50%
All extracted features (all frequency components, statistical features, and energy of 4-details wavelet analysis).	40	55%
Model 1:The variance, and the frequency components at (8.1, 8.4, 13, 17.8, 23.8, 25, 30.4, 39.2, 43.5, 44.7) Hz.	40	92.50%
Model 2: Frequency components at (8.4, 13, 18, 23.8, 25, 30.4, 39.2, 43.5) Hz.	40	80%

Table 7: The results of ANN used for classifying metal inclusion and air void defected NCIs

Feature Vector	Total Number of Testing samples (20 Air Void, 20 Metal Inclusion)	Average Classification Rate
All extracted features (all frequency components, statistical features, and energy of 4-details wavelet analysis).	40	62.50%
Model 1: The frequency components at (18.7, 19.2, 20.7, 24.4, 39.2, 43.5, 44.6, 47.8) Hz	40	95%
Model 2: Variance, and the frequency components at (19.2, 24.4, 25.3, 39.2, 43.5, 44.6, 47.8) Hz	40	87.50%

As can be noticed from the results in Table 6, feature vectors (i.e. energy of wavelet details, frequency spectrum, or statistical features) did not give good detection rates. Besides, combining all the extracted features showed low percentage classification rate. This is due to the redundant features that were confusing the function of the neural network. After that, the reduced model features found by the stepwise regression were examined by ANN. As expected, both model features gave good classification rates. Since the first model has more statistical significance than the second model, the first model gave better classification rates. As a result, ANN was able to classify between defected and non defected samples with a classification rate of 92.5%. In addition to that, the results in Table 7 show that ANN successfully classified between air void defects and metal inclusion defects where the percentage classification rate reached 95%.

3.6.2 Classification for Fibreglass Core Defects

In this part, our aim is to classify between defected and non defected fibreglass core samples as explained in the ANN results of Table 8. In addition to that, one of our targets is to specify the defect type in the fibreglass core as shown in Table 9.

Table 8: The results of ANN used for classifying defected and non defected fiberglass core samples

Feature Vector	Total Number of Testing samples (20 non defected, 20 defected)	Average Classification Rate
All extracted features (all frequency components, statistical features, and energy of 4-details wavelet analysis).	40	57.50%
Model1: Frequency Components at (2, 2.5, 3.25, 3.75, 4.25, 5.25,7,10,17.5, 17.75,20) Hz	40	90%
Model2: Frequency Components at (3.25, 3.9, 4.1 4.25, 5.25,7.2,18.5, 19.2, 21.3) Hz	40	85%

Table 9: The results of ANN used for classifying between cracked and air void defected fiberglass core samples

Feature Vector	Total Number of Testing samples	Average Classification Rate
All extracted features (all frequency components, statistical features, and energy of 4-details wavelet analysis).	40	67.50%
Model1: Frequency Components at (2.75, 4.25, 6, 7.24, 7.5, 7.75, 9.25, 9.5, 12.498)	40	97.50%
Model2: Frequency Components at (2.1, 2.75, 4.25, 6, 7.24, 9.25, 9.5, 15)	40	82.50%

As can be illustrated in Table 8, ANN was able to differentiate between defected and non defected samples where the percentage classification rate was 90%. Similar to the case of silicone rubber layer defects, using all the features to differentiate between defected and non defected fibreglass core samples will not efficiently work. Moreover, the results noticed in Table 9 show the success in differentiating between the crack and the air void in the fiberglass core where ANN reached a classification percentage of 97.5%. Moreover, the first model has terms with more statistical significance than the second model as can be observed in Table 5. So, it is only logical to expect more percentage classification rate with the first model.

3.7 Standoff Distance Effect

In all previous results, the standoff distance between the sensor and the NCI sample under test was taken to be 1mm. In this section, the effect of increasing the standoff distance to 3mm will be studied and compared with the results in Table 6. The ANN results for classification between defects (in the silicone rubber layer) and no defected samples at a standoff distance of 3mm are illustrated in Table 10.

Table 10: Classification between defects in the silicone rubber and non defected samples at standoff distance of 3mm

Feature Vector	Total Number of Testing samples (20 non defected, 20 defected)	Average Classification Rate
All extracted features (all frequency components, statistical features, and energy of 4-details wavelet analysis).	40	50%
Model 1:The variance, and the frequency components at (8.1, 8.4, 13, 17.8, 23.8, 25, 30.4, 39.2, 43.5, 44.7) Hz.	40	85.0%
Model 2: Frequency components at (8.4, 13, 18, 23.8, 25, 30.4, 39.2, 43.5) Hz.	40	72.50%

The classification rates shown in Table 10 are less than the rates in Table 6. When increasing the standoff distance, the effect of the defect on the sensor's signal will be minimized more than the effect of the moulding line. As a result, higher classification rates at a smaller standoff distance can be achieved.

3.8 3-D Scan of Different Defects

In this section, a 3-D scan to the region between two adjacent sheds was performed. All the signals, which were acquired from the scanned region, were filtered (low pass and notch filtered) and amplified. Then, the 3-D image was formed. Figure 3-18 is a 3-D scan of an air void defect.

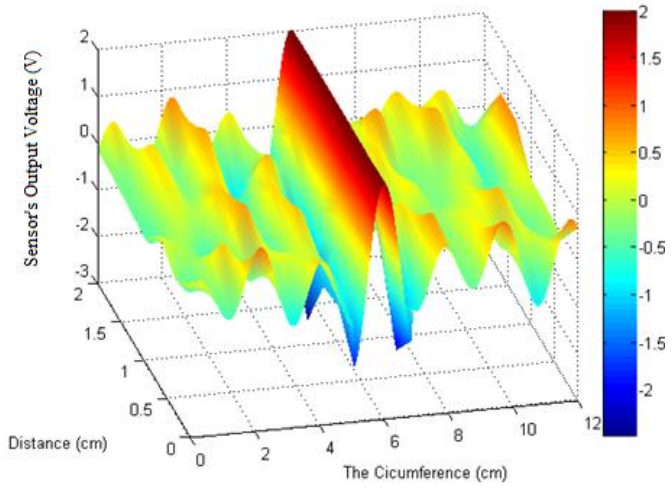

Figure 3-18: 3-D scan for a drill hole inside the silicone rubber layer

The 3-D scan shown in Figure 3-18 can help us identifying the location of the air void and distance of its extension. The air void amplitude is not high because there is no big difference between the permittivity of the silicone rubber and air.

Although the air void size does not exceed 1mm, the 3-D scan shows a 2 cm air void. It is because the 3-D scan senses the air void from the moment the open-ended waveguide sensor starts to overlap with the defect till it completely leaves it. So the defect will appear for the whole width of the waveguide.

After that, the 3-D scan of a metal inclusion in the silicone rubber layer is shown in Figure 3-19. The metallic needle was inserted at the same location of the air void.

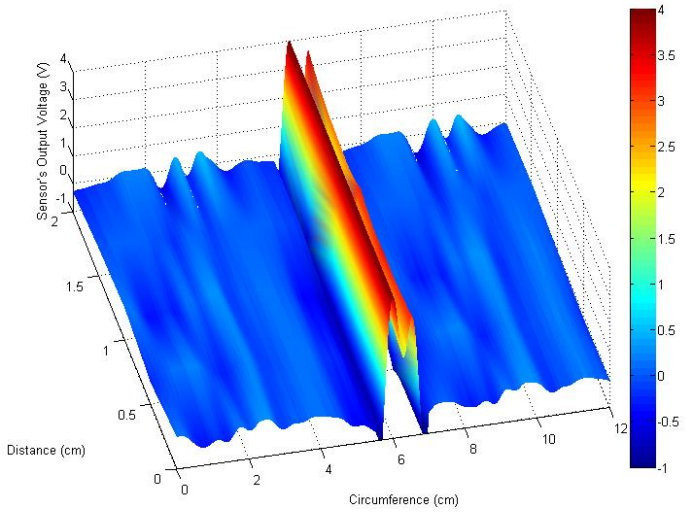

Figure 3-19: 3-D scan of metal inclusion in the silicone rubber layer

As can be noticed, there is big difference in the output voltage between the metal inclusion area and other areas. Metals usually have high imaginary permittivity value causing the reflection of a big portion of the incident energy. Hence, big difference in amplitude will be noticed. At the end, a 3-D scan for a crack in the fiberglass core is demonstrated in Figure 3-20. The 3-D scan shown in Figure 3-20 is a result of the irregularity in the internal surface of the fiberglass core. Where, the different depths of the crack along the core will vary the peaks of the reflected signal.

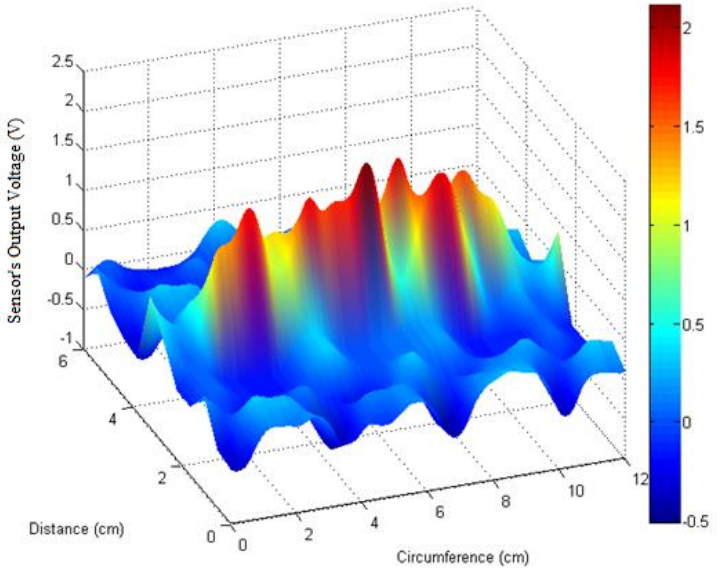

Figure 3-20: 3-D scan for a crack in the fiberglass core

CHAPTER 4: Conclusions and Recommendations for Future Work

4.1 Detection and Classification for Silicone Rubber Defects

In this work, our main focus was to develop an offline reliable testing method for internal defects in non ceramic insulators (NCIs). During the curing of the silicone rubber, an air void or metallic particles may be included in the silicone rubber matrix. In this work the use of near-field microwave signal is proposed to detect and identify two types of defects. The signal that was acquired from the near-field microwave sensor included noise. As a result, a low pass and a notch filter were used in removing the noise. However, there was still noise in our signal due to mechanical vibration during rotation and also due to the moulding line in the silicone rubber insulator. So, stepwise regression was used in extracting the important features that will be the input of the ANN. A detection rate of 92.5% was obtained.

Since it is known that the permittivity of the defect will influence the reflected signal, it was decided to work more on specifying the type of the defect. Likewise, stepwise regression is used in knowing the important frequencies that will help us differentiating between air void and metallic particles defects. As a result ANN achieved a 95% classifying rate between these two types of defects.

4.2 Detection and Classification for Fiberglass core Defects

The manufacturing process of fibreglass core is prior to the manufacturing of the NCI. Hence, it is can be exposed to many defects like crack or air void inclusion. At the beginning, ANN was able to differentiate between defected and non defected fibreglass core to a classification rate of 90%. In addition to that, ANN was able to differentiate between cracked core and air void included core samples with a classification rate of 97.5 %.

4.3 Recommendations and Future Work

A more reliable mechanical system with aligned rotation and less vibration can help a lot in minimizing the noise in the sensor's output voltage. Moreover, big quantities of real life defects will add more reliability to the training process of our ANN. Furthermore, using a Ka band sensor will increase the sensitivity and the resolution of the system. In addition to that, trying more artificial intelligent techniques like Hidden Markov Model (HMM) and polynomial neural network will certainly add more analysis to the work and will guarantee the use of the most efficient artificial intelligent technique.

References

[1] R. S. Gorur, E. A. Cherney and J. T. Burnham, *Outdoor Insulators*, Ravi. S. Gorur, Inc., 1999.

[2] A. H. El-Hag, "Effect of Insulator Profile on Aging Performance of Silicone Rubber Insulators," Ph.D. Dissertation, University of Waterloo, Waterloo, ON, Canada, 2003.

[3] B. N. Pinnangudi, R. S. Gorur and C. D. Poweleit, "Characterization of Field-Aged Nonceramic Insulators", *Annual Report Conference on Electrical Insulation and Dielectric Phenomena*, 2005, pp. 22-25.

[4] A. R. Chughtai, D. M. Smith, L. S. Kumosa, M. Kumosa, "FTIR Analysis of Non-ceramic Composite Insulators," *IEEE Trans. on Dielectrics and Electrical Insulation*, vol. 11, no. 4, pp. 585596, Aug. 2004.

[5] **"** Description and Procedure of Tests for Composite Insulators," Internet: http://www.ceramic-insulator.com/list1.asp?id=291, March 28, 2009 **[**March 18, 2010].

[6] K. L. Wong, "Electromagnetic Emission Based Monitoring Technique for Polymer ZnO Surge Arresters," *IEEE Transactions on Dielectrics and Electric Insulation*, Vol. 13, pp. 181-190, 2006.

[7] N. Qaddoumi, A. H. El-hag, M. Al Hosani, I. Al Mansouri and H. Al Ghufli "Detecting Defects in Outdoor-Non Ceramic Insulators using Near-Field Non Microwave destructive Testing," *IEEE Transactions on Dielectrics and Electric Insulation*, Vol. 17, No 2, pp. 402-407, April 2010.

[8] N. Qaddoumi, "Microwave Detection and Characterization of Subsurface Defect Properties in Composites Using Open Ended Rectangular Waveguide," Ph.D. Dissertation, Colorado State University, Fort Collins, Colorado, United States of America, 1998.

[9] S. Bakhtiari, N. Qaddoumi, S. Ganchev, and R. Zoughi "Microwave Noncontact Examination of Disbond and Thickness Variations in Stratified Composite Media," *IEEE Transactions on Microwave Theory and Techniques*, vol. 42, pp. 389-395, March 1994.

[10] A. Bin Sediq, N. Qaddoumi "Near-Field Microwave Image Formation of Defective Composites Utilizing Open-Ended Waveguides with Arbitrary Cross Section," *Journal of Composite Structure*, vol. 71, pp. 343-348, 2005.

[11] N. Qaddoumi, W. M.Saleh, M. Abu-Khousa "Innovative Near-Field Microwave Non Destructive Testing of Corroded Metallic Structure Utilizing Open-Ended Waveguide Probes," *IEEE Transaction on Instrumentation and Measurement*, vol. 56, no. 5, pp. 1961-1966, 2007.

[12] S. R. Pennock, and P. R. Shepard, *Microwave Engineering with Wireless Applications*, London: Macmillan Press LTD Hound Mills, 1998.

[13] R. G. Lyons, *Understanding Digital Signal Processing*, 2nd ed., Prentice Hall, 2004.

[14] D. W. Stockburger (1996, July 7), *Introductory Statistics: Concepts, Models, and Applications*, [Online] Available: http://www.psychstat.missouristate.edu/introbook/sbk00.htm [2011, Feb. 3].

[15] N. Shaphard, *Stochastic Volatility: Selected Readings*, Oxford University Press, 2005.

[16] Math works, Statistical Toolbox User Guide, 2008.

[17] G. Strang and T. Nguyen, *Wavelet and Filter Banks*. Wellesley, MA: Wellesley-Cambridge Press, 1997.

[18] L. M. Bruce, C. H. Koger, and J. Li "Dimensionality Reduction of Hyper spectral Data Using Wavelet Transform Feature Extraction", *IEEE Transactions On Geoscience and Remote Sensing*, Vol. 40, No.10 , pp. 2331-2339, 2002.

[19] D. Montgomery, G. Ruger, *Applied Statistics and Probability for Engineers*, NJ: Wiley, 1994.

[20] T. Shanableh, K. Assaleh, "Feature Modeling using Polynomial Classifier and Stepwise Regression," *Neurocomputing, in press Accepted Manuscript*, March, 2010.

[21] R. O. Duda, P. E. Hart, D. G. Stork, *Pattern Classification*, 2nd ed. New York: Wiley & sons, 2001.

VITA

Yasser Adel Saker was born in Syria in 1986. He moved to United Arab Emirates (U.A.E) in 1994 where he continued his schooling education. In 2004, he finished his high school education holding tenth rank among U.A.E government school students with a cumulative average of 99.2 %. He received Abu Dhabi Water and Electricity Authority (ADWEA) scholarship to join Electrical Engineering program at the American University of Sharjah (AUS). Mr. Saker was awarded the Bachelor of Science certificate in Electrical Engineering from AUS with Cum Laude standing in 2008. In 2009, Mr. Saker started his Master of Science program in Electrical Engineering in AUS. He was awarded the Master of Science degree in 2011. Meanwhile, he has been working with Abu Dhabi Distribution Company (ADDC) since 2008.